



Obesity promotes fumonisin B1 hepatotoxicity

Léonie Dopavogui^{a,1}, Marion Régnier^{a,1}, Arnaud Polizzi^a, Quentin Ponchon^a, Sarra Smati^{a,b}, Wendy Klement^a, Frédéric Lasserre^a, Céline Lukowicz^a, Yannick Lippi^a, Anne Fougerat^a, Justine Bertrand-Michel^c, Claire Naylies^a, Cécile Canlet^a, Laurent Debrauwer^a, Elodie Rousseau-Bacquié^a, Laurence Gamet-Payrastre^a, Charlène Dauriat^g, Josefina Casas^{d,e}, Siska Croubels^f, Siegrid De Baere^f, Hester M. Burger^g, Benoit Chassaing^h, Sandrine Ellero-Simatos^a, Hervé Guillou^a, Isabelle P. Oswald^a, Nicolas Loiseau^{a,*}

^a Toxalim (Research Centre in Food Toxicology), Université de Toulouse, INRAE, ENVT, INP-Purpan, UPS, Toulouse, France

^b L'institut du thorax, Inserm, CNRS, Univ Nantes, CHU Nantes, Nantes, France

^c INSERM I2MC, Toulouse, France

^d Research Unit on BioActive Molecules (RUBAM), Department of Biological Chemistry, IQAC-CSIC, Barcelona, Spain

^e CIBEREHD, Madrid, Spain

^f Department of Pathobiology, Pharmacology and Zoological Medicine, Faculty of Veterinary Medicine, Ghent University, Merelbeke, Belgium

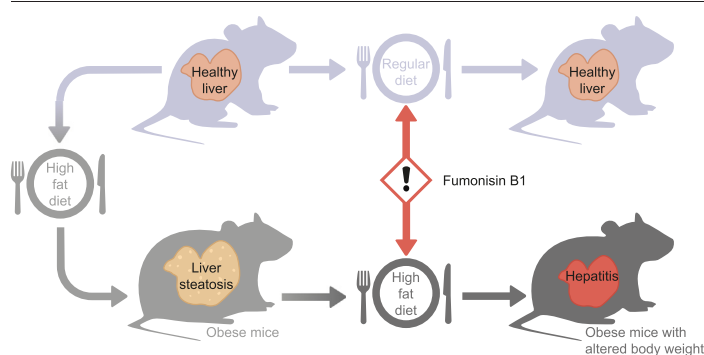
^g Unit of Research Integrity, Research Directorate, Cape Peninsula University of Technology, Bellville, South Africa

^h INSERM U1016, Team "Mucosal Microbiota in Chronic Inflammatory Diseases", CNRS UMR 8104, Université Paris Cité, Paris, France

HIGHLIGHTS

- Obese mice had altered body weight, glucose, and liver lipids when exposed to FB1.
- FB1 increased markers of hepatotoxicity in obese mice, not in regular diet mice.
- FB1 caused liver inflammation in obese mice, not in regular diet mice.
- Obesity increase toxicity of FB1 and may enhance toxicity of other food contaminants.
- Diet and metabolic status affect the health risks assessment from food contaminants.

GRAPHICAL ABSTRACT



ARTICLE INFO

Editor: Lidia Minguez Alarcon

Keywords:

Fumonisin B1

Obesity

Steatosis

Steatohepatitis

ABSTRACT

Obesity, which is a worldwide public health issue, is associated with chronic inflammation that contribute to long-term complications, including insulin resistance, type 2 diabetes and non-alcoholic fatty liver disease. We hypothesized that obesity may also influence the sensitivity to food contaminants, such as fumonisin B1 (FB1), a mycotoxin produced mainly by the *Fusarium verticillioides*. FB1, a common contaminant of corn, is the most abundant and best characterized member of the fumonisins family. We investigated whether diet-induced obesity could modulate the sensitivity to oral FB1 exposure, with emphasis on gut health and hepatotoxicity.

Thus, metabolic effects of FB1 were assessed in obese and non-obese male C57BL/6J mice. Mice received a high-fat diet (HFD) or normal chow diet (CHOW) for 15 weeks. Then, during the last three weeks, mice were exposed to these diets in combination or not with FB1 (10 mg/kg body weight/day) through drinking water.

As expected, HFD feeding induced significant body weight gain, increased fasting glycemia, and hepatic steatosis. Combined exposure to HFD and FB1 resulted in body weight loss and a decrease in fasting blood glucose level. This

Abbreviations: FB1, fumonisin b1; HFD, high fat diet; NAFLD, non-alcoholic fatty liver disease; NASH, non-alcoholic steatohepatitis.

* Corresponding author at: Toxalim UMR1331 INRAE/ENVT/INP/UPS, 180, Chemin de Tournefeuille, BP93173, 31027 Toulouse cedex 3, France.

E-mail address: nicolas.loiseau@inrae.fr (N. Loiseau).

¹ These authors contributed equally to this work.

<http://dx.doi.org/10.1016/j.scitotenv.2023.164436>

Received 21 March 2023; Received in revised form 20 May 2023; Accepted 22 May 2023

Available online 27 May 2023

0048-9697/© 2023 The Authors. Published by Elsevier B.V. This is an open access article under the CC BY license (<http://creativecommons.org/licenses/by/4.0/>).

co-exposition also induces gut dysbiosis, an increase in plasma FB1 level, a decrease in liver weight and hepatic steatosis. Moreover, plasma transaminase levels were significantly increased and associated with liver inflammation in HFD/FB1-treated mice. Liver gene expression analysis revealed that the combined exposure to HFD and FB1 was associated with reduced expression of genes involved in lipogenesis and increased expression of immune response and cell cycle-associated genes.

These results suggest that, in the context of obesity, FB1 exposure promotes gut dysbiosis and severe liver inflammation. To our knowledge, this study provides the first example of obesity-induced hepatitis in response to a food contaminant.

1. Introduction

The prevalence of obesity has reached 13 % of the adult population worldwide, and 39 % of the world's adult population is considered overweight (World Health Organization, 2021). Therefore, obesity is considered as an epidemic disease and represents a major public health burden worldwide. Obesity promotes many other diseases, such as type 2 diabetes, cardiovascular diseases, and non-alcoholic fatty liver disease (NAFLD). Obesity fosters disease development through a combination of metabolic changes (Cirulli et al., 2019) and chronic low-grade inflammation (Rohm et al., 2022). Indeed, NAFLD gathers a spectrum of liver disorders, ranging from simple hepatic steatosis considered benign to non-alcoholic steatohepatitis (NASH), which is characterized by lipid accumulation, hepatocyte death, inflammation, and activation of fibrogenic pathways that can lead to hepatic fibrosis, cirrhosis, liver failure, and/or hepatocellular carcinoma (Ristic-Medic et al., 2022).

Excessive lipid accumulation in the liver is known to contribute to hepatic insulin resistance by generating bioactive lipid intermediates, including ceramides, which are thought to play an important role in the development of hepatic insulin resistance by affecting the insulin signaling pathway (Hage Hassan et al., 2014). Increased serum and tissue ceramide levels have been observed in mice with genetic or diet-induced obesity (Samad et al., 2006; Holland et al., 2007) and in mouse models of non-alcoholic steatohepatitis (NASH) (Montandon et al., 2019). Studies using various animal models have demonstrated that de novo ceramide synthesis plays a pathogenic role in NAFLD by inducing insulin resistance, increasing oxidative stress, promoting apoptosis, and ultimately leading to steatosis, inflammation, and fibrosis (Longato et al., 2012; Raichur et al., 2019). Finally, studies have reported that ceramides accumulate in serum and metabolically active tissues such as the liver in individuals with NAFLD (Hajduch et al., 2021; Luukkonen et al., 2016) and in nonhuman primates (Brozinick et al., 2013).

Obesity is highly linked to lifestyle and the environment. High-caloric-density diets and reduced physical activities are thought to play an important role in the development of this epidemic. In addition to genetic factors, many environmental factors influence obesity (Pillon et al., 2021), including xenobiotics, endocrine disruptors (Sun et al., 2022), and other food additives (Chassaing et al., 2015; Suez et al., 2014). Although there is increasing evidence that food contaminants can impact the development of obesity, very few studies have investigated the influence of obesity on the sensitivity to food contaminants.

Mycotoxins are fungal toxins that contaminate animal feed and human food worldwide; thus, they cause significant veterinary and public health issues. *Fusarium* spp. is among the most frequent of the fungal genera found in different cereal crops; it causes economic loss and food safety concerns, because it reduces the cereal yield and quality (Cano et al., 2016). Moreover, climate change has led to shifts in temperature and humidity conditions, which favor *Fusarium* dissemination (Nnadi and Carter, 2021). Fumonisin is the predominant mycotoxin produced by *Fusarium* spp., and fumonisin B1 (FB1) is the most prevalent and the most documented member of this family (Knutsen et al., 2018a). Similarly, fumonisin B2 (FB2), which lacks one hydroxy group in its chemical structure compared to FB1, is the second most common member of this family of toxins. Nevertheless, both members FB1 and FB2 should be considered as having the same toxicity due to their synergistic effects in combination (Knutsen

et al., 2018a, b; Yu et al., 2020). In 2007, the European Union set recommendations and regulations (Commission Recommendation 2006 [Ec] No 576/, 2006; Commission Regulation 2007 [Ec] No 1126/, 2007) for the maximum levels of fumonisins (sum of FB1 and FB2) allowed in animal feed (from 5 mg/kg for pig feed to 50 mg/kg for adult ruminant feed) and human foodstuffs (from 0.2 mg/kg for baby foods to 4 mg/kg for unprocessed maize).

FB1 exposure induces severe mycotoxicosis in pigs (Knutsen et al., 2018b), with diverse clinical symptoms. The most common symptoms are nephrotoxicity, hepatotoxicity (Terciolo et al., 2019), immunotoxicity (Devriendt et al., 2009; Halloy et al., 2005), and intestinal barrier function disturbances (Bouhet et al., 2006; Loiseau et al., 2007). To date, the known molecular mechanisms underlying FB1 toxicity are mostly related to its inhibitory effect on sphingolipid biosynthesis (Wang et al., 1991; Chen et al., 2021). Indeed, FB1 and sphingoid long-chain bases share similar structural backbone features. The inhibition of ceramide synthase increases free sphinganine levels and reduces the abundance of complex sphingolipids and ceramides (Loiseau et al., 2007). This effect results in elevating the ratio of free sphingoid bases (sphinganine/sphingosine, Sa/So) in several tissues (e.g., liver and intestine), in plasma, and in cell lines (Grenier et al., 2012; Riley et al., 1993). Moreover, previous studies from our group showed that sphingolipid metabolism and FB1 had a significant influence on lipid metabolism. Indeed, experiment with pigs exposed to FB1-contaminated diet (10 mg/kg) during 4 weeks highlights the involvement of the phosphoinositide 3-kinase (PI3K)/Protein Kinase B (AKT) / protein phosphatase 2 (PP2A) and tensin homolog (PTEN) – a common lipid metabolism regulating pathway- at the intersection of the FB1-modulated pathways (Régnier et al., 2017; Régnier et al., 2019a, b).

Therefore, the current study aimed to investigate the effect of obesity on FB1 toxicity. Thus, we fed mice a high-fat diet (HFD) to induce obesity in vivo. Next, we investigated the systemic effects through the evolution of the gut microbiota ecology balance and the hepatic responses to FB1 exposure, in both normal-weight and obese mice.

2. Materials and methods

2.1. Animals, diet, and exposure to FB1

All experiments were carried out in accordance with the European Guidelines for the Care and Use of Animals for Research Purposes. The animal study protocol was approved by an independent ethics committee (CEEA-86 Toxcométhique) under the authorization number 2016070116429578. The animals were treated humanely with due consideration to the alleviation of distress and discomfort. Mouse housing was controlled for temperature (21–23 °C) and light (12 h light/12 h dark). A total of 48 C57BL/6J male mice (6 weeks old) were purchased from Charles Rivers Laboratories (L'Arbresle, France). Mice were allowed two weeks of acclimatization with free access and ad libitum water and food, with a standard rodent diet (safe 04 U8220G10R) from SAFE (Augsy, France). Then, mice were randomly divided into four groups of 12 mice each. Two groups ($n = 24$, 4 cages of 6 mice) were fed a chow diet with 10 kcal% fat (CHOW, D12450J, Research Diets) and the other two groups ($n = 24$, 4 cages of 6 mice) were fed a high-fat diet with 60 kcal% fat (HFD, D12492, Research Diets) for 15 weeks. After 12 weeks of feeding, half of the CHOW ($n = 12$, 2 cages of 6 mice) and HFD ($n = 12$, 2 cages of 6 mice) groups were

exposed to FB1 (10 mg/kg bw/day) by adjusting every two days the amount of consumed FB1 in the drinking water during 3 weeks in order to maintain a constant level of exposure. Every week, mice were weighed, and water consumption was measured to adjust the quantity of FB1 in the water. Food intake was also monitored. At the end of the experiment, mice were sacrificed to collect plasma and tissue samples.

2.2. Blood and tissue sampling

After 15 weeks of feeding, mice were fasted for 6 h, and blood glucose levels were measured from the tail vein with an AccuCheck Performa glucometer (Roche Diagnostics). At the end of the experiment, blood was collected into EDTA-coated tubes (BD Microtainer, K2E tubes) from the submandibular vein. Plasma was isolated by centrifugation ($1500 \times g$ for 10 min at 4°C) and stored at -80°C until use for plasma biochemistry. All mice were sacrificed on the day 104 in the fed state. Following sacrifice by cervical dislocation, liver and caecum were removed, weighed, prepared for histology analysis or snap frozen in liquid nitrogen and stored at -80°C .

2.3. Plasma FB1 analysis

Equal volumes of plasma of 4 individual mice from each group were pooled and $100 \mu\text{l}$ was used for analysis. Considering this pooling of samples, only 3 FB1 level analysis have been performed per group. Plasma FB1 was analyzed with a validated UPLC-MS/MS (ultra-performance liquid chromatography-tandem mass spectrometry) method previously described (De Baere et al., 2018). The FB1 analytical standard was provided by Fermentek Ltd. (Jerusalem, Israel). The limit of quantification was determined at 0.5 ng/ml , using $100 \mu\text{l}$ of plasma. The limit of detection, corresponding to a signal-to-noise value of 3/1, was 0.09 ng/ml .

2.4. Biochemical analyses

We analyzed the following plasma constituents: alanine aminotransferase (ALT), aspartate aminotransferase (AST), alkaline phosphatase (ALP), bilirubin, creatinine, triglycerides, total cholesterol, high density lipoprotein, and low-density lipoprotein cholesterol. All biochemical analyses were performed with a COBASMIRA+ by the Anexplo technical platform team (Genotoul, Toulouse).

2.5. Lipid extraction and analysis

Liver samples were homogenized in Lysing Matrix D tubes with 1 ml of methanol/5 mM EGTA (2:1 v/v) in a FastPrep machine (MPBiochemicals). Lipids corresponding to an equivalent of 2 mg of tissue were extracted according to Bligh and Dyer, in chloroform/methanol/water (2.5:2.5:2, v/v/v), in the presence of the following internal standards: glyceryl trionadecanoate, stigmaterol, and cholesteryl heptadecanoate (Sigma, Saint-Quentin-Fallavier, France). Total lipids were suspended in $160 \mu\text{l}$ ethyl acetate, and the triglycerides, free cholesterol, and cholesterol ester components were analyzed with FID gas-chromatography on a focus Thermo Electron system with a Zebtron-1 Phenomenex fused-silica capillary column (5 m, 0.32 mm i.d. , $0.50 \text{ mm film thickness}$). The oven temperature was programmed to increase from 200 to 350°C at a rate of $5^\circ\text{C}/\text{min}$, and the carrier gas was hydrogen (0.5 bar). The injector and the detector were at 315°C and 345°C , respectively.

Liver ceramide, sphingomyelin, sphingosine, and sphinganine were extracted, as previously described (Barbacini et al., 2019), with chloroform/water/methanol (2.5:1:5 v/v/v) in the presence of the following internal standards: ceramide d18:1/12:0 (16 ng), sphingomyelin d18:1/12:0 (16 ng), sphingosine 17:0, and sphinganine 17:0 and sphingosine-1-phosphate 17:0. Sphingolipids and internal standards were analyzed by liquid chromatography mass spectrometry (LC-MS) with an Acquity ultra high-performance liquid chromatography (UHPLC) system (Waters, USA) connected to a Time of Flight (LCT Premier XE, Waters, USA) Detector or a

triple quadrupole mass spectrometer (Xevo, Waters, USA). The final data were calculated as pmol/mg of protein.

2.6. Proton nuclear magnetic resonance ($^1\text{H NMR}$)-based metabolomics

$^1\text{H NMR}$ spectroscopy was performed on aqueous liver extracts prepared from liver samples ($50\text{--}75 \text{ mg}$). Briefly, livers were homogenized in chloroform/methanol/NaCl 0.9 % (2/1/0.6, v/v/v) containing 0.1 % butyl hydroxytoluene. Homogenates were centrifuged at $5000 \times g$ for 10 min. The supernatant was collected, lyophilized, and reconstituted in $600 \mu\text{l}$ of D_2O that contained 0.25 mM 3-(trimethylsilyl) propionic-(2,2,3,3- d_4) acid sodium salt (TSP), as a chemical shift reference at 0 ppm.

All $^1\text{H NMR}$ spectra were obtained on a Bruker DRX-600-Avance NMR spectrometer (Bruker) equipped with the AXIOM metabolomics platform (MetaToul). The instrument was operated at 600.13 MHz for ^1H resonance frequency. It included an inverse detection $5\text{-mm } ^1\text{H}\text{-}^{13}\text{C}\text{-}^{15}\text{N}$ cryoprobe attached to a cryoplatfrom (the preamplifier cooling unit).

$^1\text{H NMR}$ spectra were acquired at 300 K with a standard, one-dimensional noesypr1D pulse sequence with water presaturation and a total spin-echo delay (2 ns) of 100 ms. Data were analyzed by applying an exponential window function with a 0.3-Hz line broadening, prior to Fourier transformation. The resulting spectra were phased, baseline-corrected, and calibrated to TSP (0.00 ppm) manually with Mnova NMR (version 9.0; Mestrelab Research S.L.). The spectra were subsequently imported into MatLab (R2014a; MathWorks, Inc.). All data were analyzed with the use of full-resolution spectra. The $^1\text{H NMR}$ peak assignments of aqueous phase extracts from liver are presented in Supplementary Table 2. The region containing the water resonance ($4.6\text{--}5.2 \text{ ppm}$) was removed, and the spectra were normalized to the probabilistic quotient (Dieterle et al., 2006) and aligned with a previously published function (Veselkov et al., 2009).

Data were mean-centered and scaled with unit variance scaling, prior to performing orthogonal projection on latent structure-discriminant analysis (O-PLS-DA). The O-PLS derived model was evaluated for accuracy of prediction (Q²Y value) with 10-fold cross-validation. The parameters of the final models are indicated in the figures. Metabolite identifications and discriminations between the groups were performed by calculating the O-PLS-DA correlation coefficients (r^2) for each variable, and then, back-scaling into a spectral domain to preserve the shapes of the NMR spectra and the signs of the coefficients (Cloarec et al., 2005). The weights of the variables were color-coded, according to the square of the O-PLS-DA correlation coefficients.

Correlation coefficients extracted from significant models were filtered, and only significant correlations above the threshold defined by Pearson's critical correlation coefficient ($p < 0.05$; $r^2 > 0.55$; for $n = 12$ per group) were considered significant. For illustration purposes, the areas under the curves of several signals of interest were integrated, and significance was tested with a univariate test.

2.7. Histology

Hematoxylin/eosin (H&E) staining was performed on paraformaldehyde-fixed, paraffin-embedded liver tissue sections ($3 \mu\text{m}$). Sections were visualized with a Leica DFC300 camera. Livers were examined with light microscopy. First, liver sections were screened to determine all the effects present on each section. The histological features were grouped with the steatosis score (evaluated according to Contos et al., 2001). Liver sections were evaluated for steatosis and inflammation. The steatosis score was based on the percentage of vacuoles surface in hepatocytes that contained fat, where Grade 0 = no hepatocytes containing fat in any section; grade 1 = 1 % to 25 % of hepatocytes; grade 2 = 26 % to 50 % of hepatocytes; grade 3 = 51 % to 75 % of hepatocytes; and grade 4 = 76 % to 100 % of hepatocytes. The inflammation score was the number of inflammatory foci counted in 10 distinct $200 \times$ fields for each liver section. Values represented the mean of 10 fields/liver section.

2.8. Gene expression studies

Total cellular RNA was extracted with Trizol reagent (Invitrogen). Transcriptome profiles were performed with the Agilent Whole Mouse Genome microarray (4 × 44 K), according to manufacturer instructions. Microarray data and all experimental details are available in the Gene Expression Omnibus Series database (accession number GSE208735; <https://www.ncbi.nlm.nih.gov/geo/query/acc.cgi?acc=GSE208735>).

Total RNA samples (2 µg) were reverse-transcribed with the high-capacity cDNA reverse transcription kit (Applied Biosystems), then analyzed with real-time quantitative polymerase chain reaction (qPCR). Primers for the Sybr Green assays are presented in Supplementary Table 1. Amplifications were performed on a Stratagene Mx3005P thermocycler (Agilent Technology). qPCR data were normalized to the endogenous level of proteasome 20S subunit beta 6 messenger RNA (mRNA) and analyzed with LinRegPCR software.

2.9. Microbiota composition analysis through 16S rRNA gene sequencing

We performed 16S ribosomal RNA (rRNA) gene amplification and sequencing with Illumina MiSeq technology, according to the protocol described by the Earth Microbiome Project, with slight modifications (www.earthmicrobiome.org/emp-standard-protocols). Briefly, frozen extruded feces samples were mechanically disrupted (bead beating), and DNA was extracted with a PowerSoil-htp kit (QIAGEN). From each DNA sample, the 16S rRNA genes from region V3-V4 were PCR-amplified with a composite forward primer and a reverse primer. The reverse primer contained a unique 12-base barcode, designed with the Goyal error-correcting scheme, which was used to tag PCR products from respective samples. The composite forward 515F primer sequence was: 5'-AATGATACGGCGACCACCGAG ATCTACAGCCTXXXXXXXATGTTAATTGTGTGTCAGCGMGGCCG CGGTAA-3' where the italicized sequence is the 5' Illumina adaptor, the 12 X sequence is the goyal barcode, the bold sequence is the primer pad, the italicized and bold sequence is the primer linker, and the underlined sequence is the conserved bacterial primer 515F. The reverse primer 806R used was 5'-CAAGCAGAAGACGGCATACGAGATAGTCAGCCAGCCGGAC TACNVGGGTWTCTAAT-3' where the italicized sequence is the 3' reverse complement sequence of Illumina adaptor, the bold sequence is the primer pad, the italicized and bold sequence is the primer linker and the underlined sequence is the conserved bacterial primer 806R. PCR reactions consisted of Hot Master PCR mix (Quantabio, Beverly, MA, USA), 0.2 mM of each primer, 10–100 ng template, and reaction conditions were 3 min at 95 °C, followed by 35 cycles of 45 s at 95 °C, 60 s at 50 °C and 90 s at 72 °C on a Biorad thermocycler. PCR products were quantified using Quant-iT PicoGreen dsDNA assay on a BIOTEK Fluorescence Spectrophotometer and a master DNA pool was generated from the purified products in equimolar ratios. The obtained pool was purified with Ampure magnetic purification beads (Agencourt, Brea, CA, USA), and visualized by gel electrophoresis and then sequenced using an Illumina MiSeq sequencer (paired-end reads, 2 × 250 bp) at the GenomIC platform from Cochin Institute.

2.10. 16S rRNA gene sequence analysis

16S rRNA sequences were analyzed with QIIME2 – version 2019.360 (Bolyen et al., 2019). Sequences were demultiplexed and quality-filtered with the Dada2 method (Callahan et al., 2016). We used QIIME2 default parameters to detect and correct Illumina amplicon sequence data, and a table of Qiime 2 artifacts was generated. Next, a tree was generated with the align-to-tree-mafft-fasttree command, for analyzing phylogenetic diversity. Then, alpha and beta diversity analyses were computed with the core-metrics-phylogenetic command. We constructed principal coordinates analysis (PCoA) plots to assess the variation between experimental groups (beta diversity). To analyze the taxonomy, we assigned features to operational taxonomic units, according to a 99 % threshold of pairwise identity to the Greengenes reference database 13.8. Unprocessed sequencing data

are deposited in the European Nucleotide Archive under accession number PRJEB54776, publicly accessible at <https://www.ebi.ac.uk/ena/browser/view/PRJEB54776>.

2.11. Statistical analysis

Gene expression measurement by qPCR and sphingolipid quantification data were log₂ transformed and analyzed using R (<http://www.r-project.org>). If a significant difference ($p < 0.05$) was detected by ANOVA, Welch test were conducted to compare the groups means. Benjamini-Hochberg correction was applied over all variates for each comparison. An adjusted p -value < 0.05 was considered significant.

Hierarchical clustering of microarray gene expression data was performed with the R packages, Geneplotter and Marray (<https://www.bioconductor.org/>). We used Ward's algorithm, modified by Murtagh and Legendre, as the clustering method. Comparisons were performed with ANOVAs. All data represented on heat maps had p -values < 0.05 for one or more comparisons.

Statistical analyses of microbiota data, lipid quantification, phenotypical and biochemistry data were performed with GraphPad Prism for Windows (GraphPad Prism 7.03). When one-way or two-way ANOVAs found statistically significant differences, they were followed by the appropriate posthoc test (Tukey). Comparisons between two groups were performed with the student's t -test. P -values < 0.05 were considered significant.

3. Results

3.1. FB1 exposure attenuates the effect of HFD feeding on body weight and fasting glycemia

Eight-week-old C57BL/6J male mice were either fed a low-fat chow diet (10 % fat, CHOW) or a HFD (60 % fat) ad libitum for 15 weeks. At the beginning of the experiment, the four groups of mice were homogeneous in terms of weight. The two groups of mice fed the HFD became overweight within 12 weeks and gained an average of 2 g body weight (bw) per week per mouse (Fig. S1A). During the same time period, the two groups of mice fed the CHOW diet only gained 0.33 g body weight (bw) per week per mouse for a total of 4 g of body weight increase per mouse within the 12 weeks (Fig. 1A). HFD-fed mice gained significantly more weight, starting from the second week of HFD feeding (Fig. 1A). The difference in body weight continued until the 12th week, when half the mice in each group were exposed to FB1. Thus, during the last three weeks, FB1 (10 mg/kg bw/day) was only added to the drinking water of FB1-exposed groups. From the 12th week to the end of the experiment, FB1 exposure did not affect the weight of CHOW-fed mice, but it induced significant weight loss in HFD-fed mice (around 5 g per mouse; Figs. 1A and S1B). An evaluation of the food consumed during the last 3 weeks revealed a significant reduction in daily quantity of food intake associated with the HFD in mice exposed to FB1 (but not in the energy intake that significantly increase – Fig. S1C), but FB1 did not significantly influence feeding in CHOW-fed mice (Fig. 1B). In the same period, water consumption increased in mice exposed to FB1 under the CHOW diet, but not in mice under the HFD (Fig. 1C). We checked water consumption to monitor the FB1-exposure level during the experiment and found that exposure to FB1 was similar in both dietary groups (HFD = 10.5 ± 0.2 mg/kg bw/day vs. CHOW = 10.7 ± 0.6 mg/kg bw/day; Fig. 1D).

In response to HFD feeding, we observed significant increases in the levels of fasting blood glucose and blood insulin (respectively Fig. 1E,F). However, FB1-exposed mice under the HFD had significantly lower fasting blood glucose levels than the unexposed HFD-fed mice (Fig. 1E).

Finally, since HFD diet may influence intestinal permeability (Nakanishi et al., 2021), we evaluated plasma FB1 levels to determine whether the HFD modulated the oral bioavailability of FB1 (Fig. 1G). A comparison between FB1-exposed mice fed CHOW or HFD showed that the HFD increased the FB1 plasma level by 4.5-fold, from 1.54 ± 0.2 ng/ml to 6.92 ± 0.8 ng/ml. Taken together, these results demonstrate

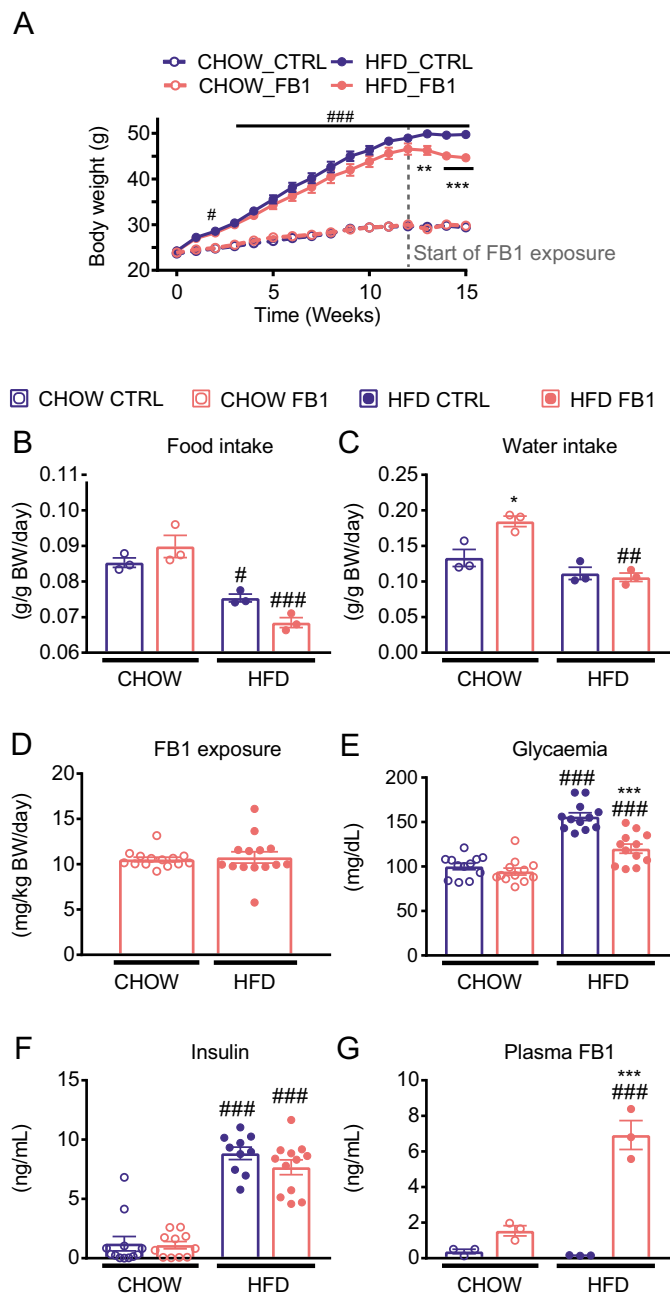


Fig. 1. FB1 exposure reverses the effect of HFD on body weight and fasting glucose. (A) Mean body weight measured weekly during the study period. (B) Average food intake during the 3 weeks of FB1 exposure. (C) Average water intake during the 3 weeks of FB1 exposure (D) Average FB1 exposure. (E) Fasting glycemia after 2 weeks of FB1 treatment. (F) Insulin levels in the fed state after 3 weeks of FB1 treatment. (G) FB1 level in the plasma. Results are the mean \pm SEM ($n = 12$ /group and each level correspond to the pooling of 4 mouse samples). # diet effect, * treatment effect. * or # p -value < 0.05 , ** or ## p -value < 0.01 , *** or ### p -value < 0.001 ; FB1: fumonisin B1; CTRL: not exposed to FB1.

that HFD-induced obesity and hyperglycemia blood level were partially reversed by FB1 exposure. This FB1 effect observed in obese mice was correlated with an increase plasma concentration of FB1.

3.2. HFD feeding and FB1 exposure influence gut microbiota composition

Next, we investigated whether FB1 effects on obesity and glycemia were related to altered gut homeostasis. We analyzed the effects of both HFD feeding and FB1 exposure on cecal microbial structure through V3-V4

hypervariable regions in 16S rRNA high throughput sequencing. Under a CHOW diet, FB1 exposure did not impacted intestinal microbiota alpha diversity while, as expected, HFD was associated with significant decrease in alpha diversity, as assessed by both the Shannon and Simpson index (Fig. 2A). Importantly, in HFD-fed mice exposed to FB1, alpha diversity was restored to levels similar to those observed in CHOW-fed mice, suggesting an impact of both HFD and FB1 in regulating intestinal microbiota composition. In order to investigate which phyla were impacted by HFD and/or FB1, we next explored the relative frequencies of taxa at the phylum level (Fig. 2B). HFD feeding significantly decreased the relative frequency of Firmicutes and Actinobacteria and increased the relative frequency of Proteobacteria. In CHOW-fed mice, FB1 did not significantly change the Proteobacteria frequency, but the Actinobacteria and the Firmicutes frequencies were significantly reduced, while the Verrucomicrobia frequency was significantly increased, compared to the frequencies observed in unexposed CHOW-fed mice. In HFD-fed mice, FB1 exposure had little or no significant effects on the relative frequencies of Actinobacteria and Firmicutes. Nevertheless, these results showed that FB1 did not have either synergistic or cumulative effects. For Proteobacteria, the HFD combined with FB1 exposure attenuated the increased relative frequency observed with the HFD alone. However, FB1 induced an increase in the frequency of the Verrucomicrobia phylum in HFD-fed mice.

Beta diversity was next evaluated using the Bray-Curtis and unweighted unifracs dissimilarity indexes (Fig. 2C–E). Both PCoA plots showed that HFD feeding was the main factor driving differences in gut microbiota composition, with a clear separation along the 1st PCoA axis (Fig. 2D–E). The Bray-Curtis PCoA plot illustrates a significant effect of FB1 in both CHOW- and HFD-fed mice. In the unweighted unifracs PCoA, the FB1-CHOW and the CTRL-CHOW groups were merged, while significant distinct clustering was observed between FB1-HFD and CTRL-HFD groups (Fig. 2E), suggesting a stronger impact of FB1 in HFD-fed mice on low abundant ASVs. These findings were confirmed by investigation of the distances separating individual animals within or between groups (Fig. 2C). The bray-curtis distance between the FB1- and CTRL-treated animals fed a CHOW diet was significantly lower than the distance between the FB1- and CTRL-treated animals fed a HFD diet, while the opposite pattern was observed using the unweighted unifracs distance (Fig. 2D). This indicates that FB1 effects on the gut microbiota seem to depend on the animal diet, with FB1 impacting mostly low abundant bacteria upon HFD feeding.

Finally, we conducted association analysis between microbial ASVs and experimental groups using general linear models (Fig. 2F–H). Upon CHOW diet, we found 14 ASVs significantly more abundant, and 16 ASVs significantly less abundant in FB1-treated vs. CTRL mice; while upon HFD diet, 29 ASVs were significantly more abundant, and 16 ASVs significantly less abundant, in FB1-treated vs. CTRL mice. Surprisingly, only 2 ASVs were significantly impacted by FB1 under both dietary regimen (Fig. 2F). Adjusted q -value-based hierarchical clustering of these significant OTUs further illustrates this diet-dependent impact of FB1 on gut microbiota, with the ASVs clearly clustering into 5 different clusters (Fig. 2G). Among those, ASVs belonging to clusters 1 and 5, illustrate a clear FB1 * diet interaction, with FB1 impacting ASVs relative abundance only in HFD-fed mice (Fig. 2H).

Taken together, these results demonstrate that HFD was the first modifying factor of gut microbiota ecological balance, while FB1 impacted gut microbiota more profoundly upon HFD- than upon CHOW diet, suggesting an interaction between HFD and FB1 on the intestinal microbiota composition.

3.3. FB1 reverses HFD-induced hepatic steatosis, but promotes liver inflammation

Next, we performed histological analyses of the liver to assess the effects of HFD feeding and FB1 exposure on liver physiology and homeostasis (Fig. 3A). Histological H&E staining showed that HFD feeding induced steatosis. In CHOW-fed mice, FB1 exposure did not induce any detectable morphological differences from unexposed samples. However, in the HFD group, FB1 exposure induced a marked reduction in steatosis compared

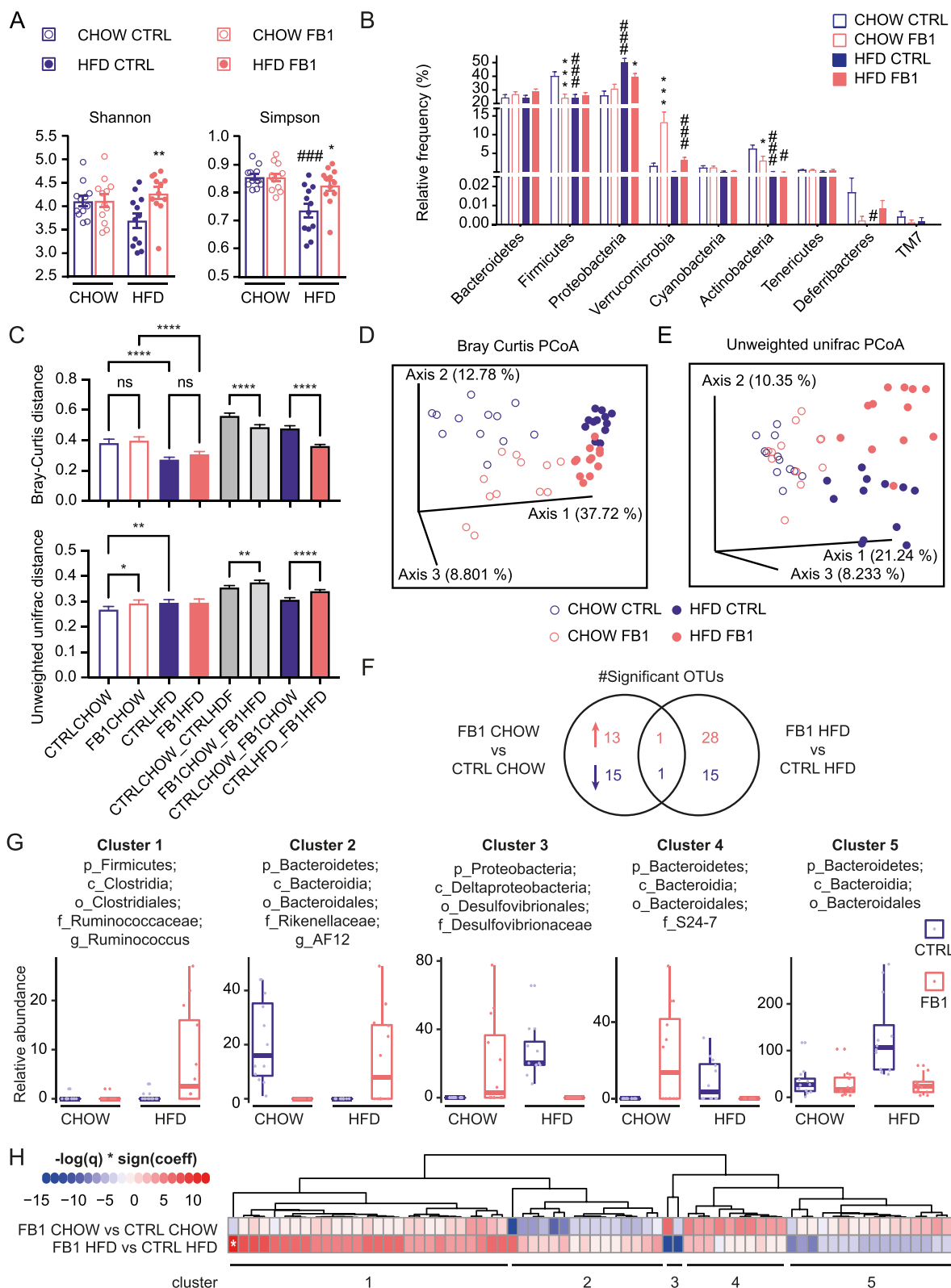


Fig. 2. FB1 effects on gut microbiota composition.

The cecal microbial composition of samples was analyzed by sequencing 16S rRNA genes. (A) Alpha diversity was assessed by calculating the Shannon and Simpson indexes. (B) Relative frequencies of taxa at the phylum level. (C) Beta diversity was assessed with the Bray-Curtis and unweighted unifrac dissimilarity indexes and distances between individuals within and between groups were compared. (D) PCoA plot of beta-diversity using the Bray Curtis index. (E) PCoA plot of beta-diversity using the unweighted unifrac index. (F) General linear models were fitted to find OTUs significantly different between the experimental groups. Venn diagram representing the number of significant OTUs higher (red) or lower (blue) in FB1- vs. CTRL groups. (G) Hierarchical clustering of the OTUs significantly different between FB1 and CTRL mice in either CHOW- or HFD-fed mice. (H) Relative abundance of one representative OTU from each cluster. Data are presented as the mean \pm SEM (n = 12/group). #diet effect, *treatment effect; * or # p-value < 0.05, ** or ## p-value < 0.01, *** or ### p-value < 0.001; FB1: Fumonisin B1; CTRL: not exposed to FB1; PCoA: principle coordinates analysis.

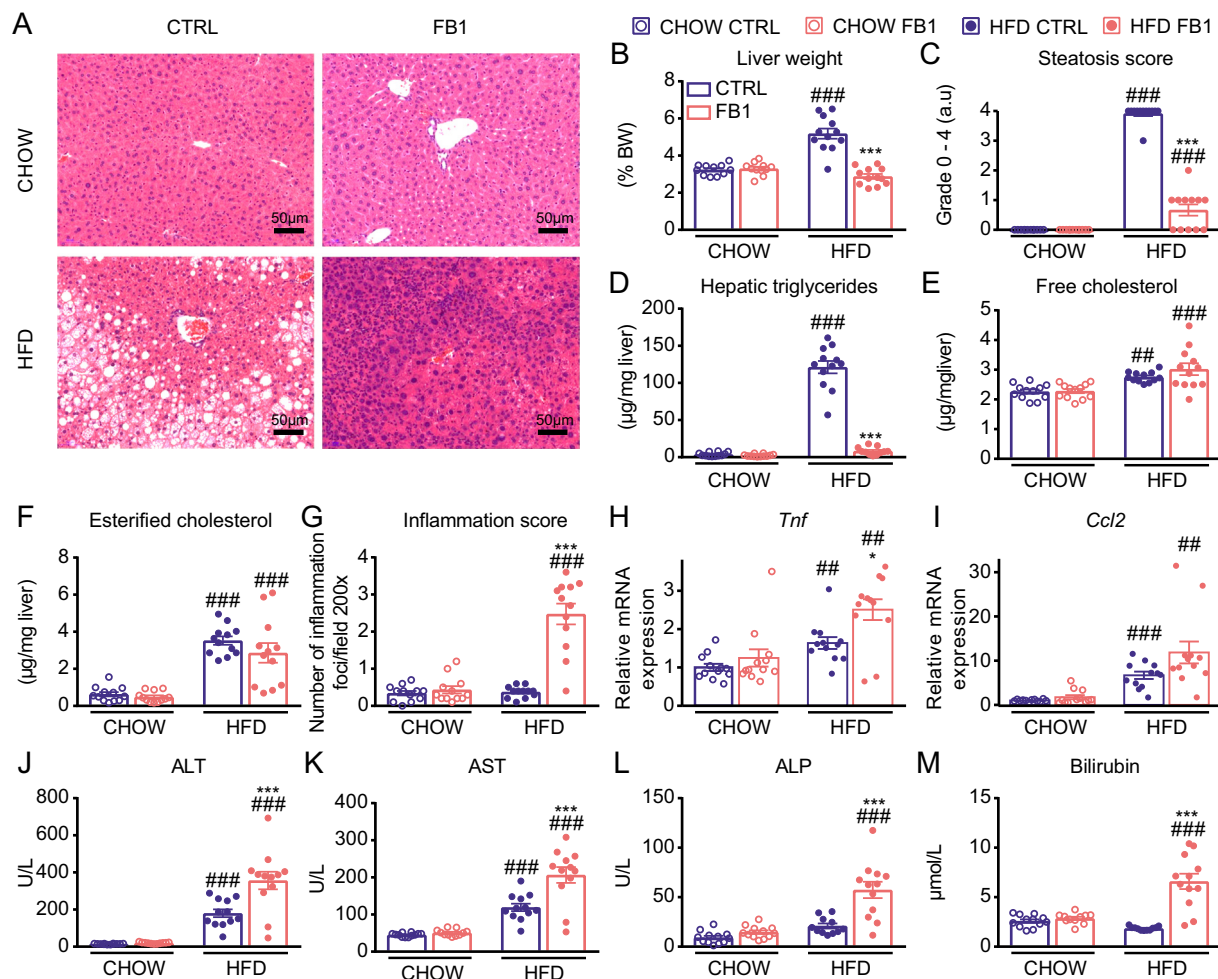


Fig. 3. FB1 reverses HFD-induced hepatic steatosis, but promotes liver inflammation.

(A) Representative histological liver sections from mice in each group stained with hematoxylin and eosin; magnification $\times 100$. Scale bars: 50 μm . (B) Average liver weight, expressed as a percentage of body weight. (C) Liver steatosis scores, estimated on liver sections ($n = 12/\text{group}$). (D–F) Lipids were extracted from livers and quantified with gas-liquid chromatography: (D) triglycerides, (E) free cholesterol, and (F) esterified cholesterol. (G) Inflammatory scores: liver sections were analyzed in 10 microscopic fields ($200\times$ magnification) to determine the mean number of inflammatory foci per field ($n = 12$ per group). (H–I) mRNA expression levels of genes that encode cytokines involved in inflammation: (H) *Tnfa* and (I) *Ccl2*. (J–M) End of experiment plasma levels of (J) aspartate aminotransferase (AST), (K) alanine aminotransferase (ALT), (L) alkaline phosphatase (ALP), and (M) bilirubin. Results are presented as the mean \pm SEM. #diet effect, *treatment effect, * or # p-value < 0.05 , ** or ## p-value < 0.01 , *** or ### p-value < 0.001 ; FB1: Fumonisin B1; CTRL: not exposed to FB1.

to the unexposed group. These results were associated with a significant decrease in liver weight (Fig. 3B), steatosis scores (Fig. 3C), hepatic triglycerides (Fig. 3D) and in some mRNA relative gene expression corresponding to lipogenesis (Fig. S2A). Additionally, both hepatic free-cholesterol and esterified cholesterol were increased in the HFD group compared to the CHOW group, but FB1 exposure did not significantly affect these HFD effects (Fig. 3E and F).

Furthermore, H&E staining revealed that liver sections from mice fed the HFD and exposed to FB1 had significantly more inflammatory foci than any of the other mouse groups (Fig. 3A). Liver inflammation was confirmed by the inflammatory score (Fig. 3G), and by some relative gene expression increase associated to inflammatory response such as *Tnf* and *Ccl2* (Fig. 3H,I); but also associated to TLR4 response, inflammasome and fibrosis (Fig. S2B,C). Although both of these genes were significantly upregulated in response to the HFD, only the relative expression *Tnf* mRNA was significantly increased with FB1 exposure, compared to HFD feeding alone (Fig. 3H,I).

Liver damage was confirmed by analyzing plasma levels of ALT (Fig. 3J) and AST (Fig. 3K). Both these enzymes were elevated in HFD-fed mice compared to CHOW-fed mice. In HFD-fed mice, FB1 exposure caused further elevations of ALT and AST. In addition, the plasma ALP and total bilirubin

levels were significantly increased when HFD-fed mice were exposed to FB1 (Fig. 3L,M).

Taken together, these data suggest that the FB1 combined with HFD reversed HFD-induced hepatic steatosis, but promoted liver inflammation and hepatocytolysis.

3.4. Effect of FB1 on hepatic sphingolipid homeostasis

With FB1 being a known ceramide synthase inhibitor, we next investigated FB1-induced alterations in hepatic sphingolipid metabolism in both CHOW-fed and HFD-fed mice. We measured several sphingolipid species in the liver, including sphinganine (Sa), sphingosine (So), sphingosine-1-phosphate (S1P), ceramides, dihydroceramides, and sphingomyelins (Fig. 4).

As expected, under the CHOW diet, FB1 exposure induced significant increases in the hepatic levels of sphingoid bases and of the Sa/So ratio (3-fold increase, Fig. 4A–C). These sphingoids are well-known biomarkers for FB1 effects (Fig. 4A–C). Moreover, the total hepatic levels of dihydrosphingomyelins also increased significantly with FB1 exposure under the CHOW diet (Fig. 4H). Surprisingly, under the CHOW diet, the level of FB1 exposure applied did not significantly affect the hepatic levels of S1P, total ceramides, total dihydroceramides, or total sphingomyelins

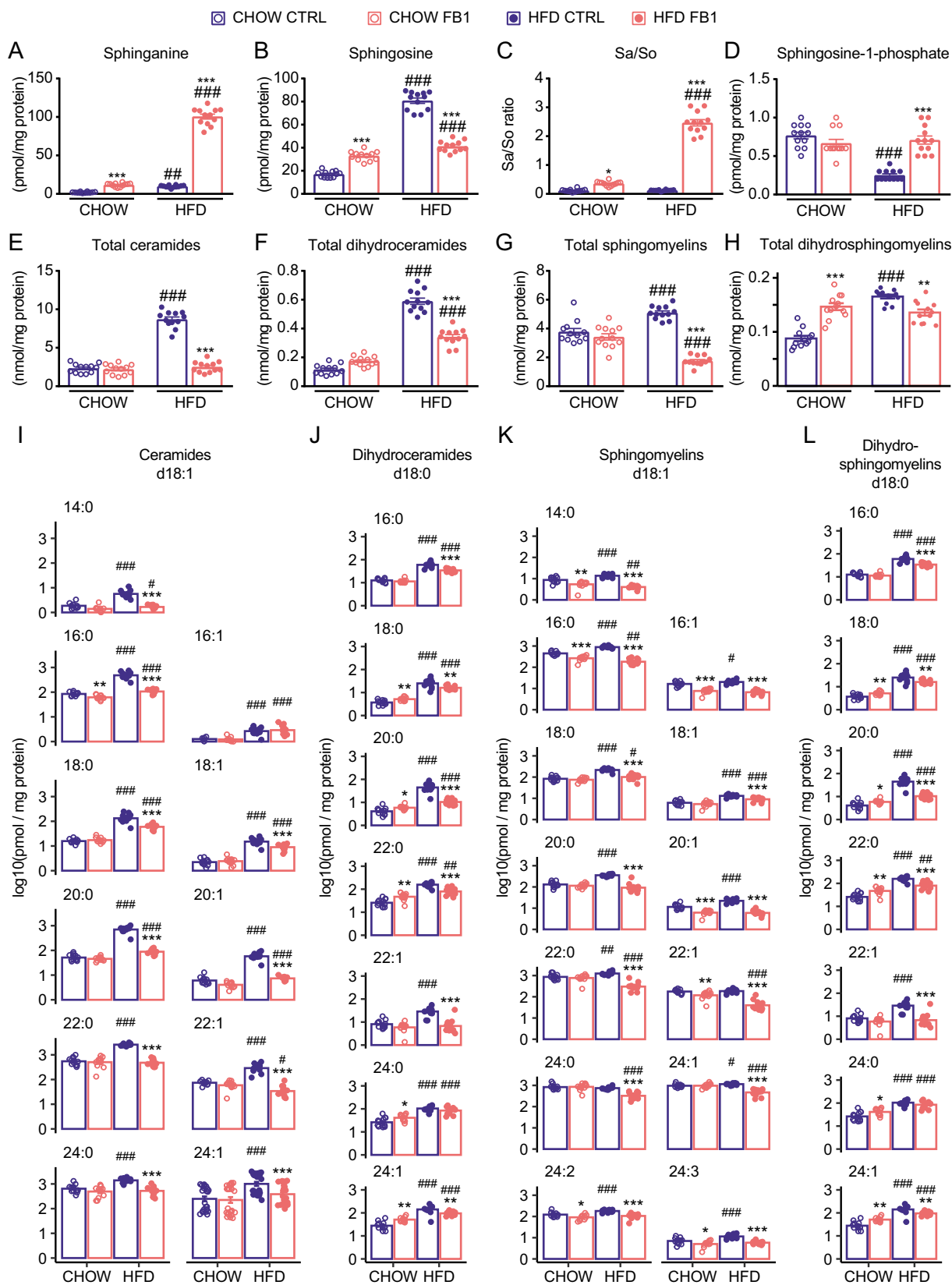


Fig. 4. FB1 effects on sphingolipid homeostasis.

Liver samples were analyzed for the levels of (A) sphinganine, (B) sphingosine, (C) the sphinganine/sphingosine ratio (Sa/So), (D) sphingosine-1-phosphate, (E) total ceramides, (F) dihydroceramides, (G) sphingomyelins, and (H) dihydrosphingomyelins. (I-L) To evaluate the abundances of sphingolipids as a function of the length of the fatty acid residue, we performed separate measurements of (I) ceramide, (J) dihydroceramide, (K) sphingomyelin, and (L) dihydrosphingomyelin species. Results are presented as the mean \pm SEM. #diet effect, *treatment effect. * or # p-value < 0.05, ** or ## p-value < 0.01, *** or ### p-value < 0.001; FB1: Fumonisin B1; CTRL: not exposed to FB1.

(Fig. 4D–G). A closer look at the specific ceramide and sphingomyelin species (Fig. 4I, K) showed that the abundances of some were significantly reduced, including ceramide(d18:1/16:0), sphingomyelin(d18:1/14:0), sphingomyelin(d18:1/16:0), sphingomyelin(d18:1/16:1), sphingomyelin(d18:1/20:1), sphingomyelin(d18:1/22:1), sphingomyelin(d18:1/24:2), and sphingomyelin(d18:1/24:3). Moreover, under the CHOW diet, FB1 exposure induced significantly higher levels of specific dihydroceramides (Fig. 4J) and long carbon-chain dihydrosphingomyelins (Fig. 4L).

Under HFD feeding, the basal hepatic levels of ceramides, dihydroceramides, sphingomyelins, and dihydrosphingomyelins significantly increased (Fig. 4E–H). Similarly, the levels of sphinganine and sphingosine increased, but the Sa/So ratio remained unchanged (Fig. 4A–C). In contrast, the level of sphingosine-1-phosphate (S1P) significantly decreased when the subjects were fed a high-fat diet (HFD) (Fig. 4D). Analyzing the specific ceramides, dihydroceramides, sphingomyelins, and dihydrosphingomyelins species, we found that HFD feeding caused significant elevations in nearly all species (Fig. 4I–L).

When the HFD was combined with FB1 exposure, stronger effects were observed on sphingolipid metabolism. This combined treatment induced a significant increase in the hepatic sphinganine levels (Fig. 4A) and a reduction in the hepatic sphingosine levels, to the level observed in unexposed HFD-fed mice, but not to the level observed in CHOW-fed unexposed mice (Fig. 4B). These changes in sphingoid base levels resulted in a marked increase in the Sa/So ratio (20-fold increase), which is characteristic of severe FB1 contamination (Fig. 4C). Moreover, when the HFD was combined with FB1 exposure, the reduced sphingosine level was associated with a significant increase in the S1P level, to the level observed in unexposed HFD-fed mice (Fig. 4D). In addition, the HFD combined with FB1 exposure caused significant reductions in the hepatic levels of ceramide, dihydroceramides, sphingomyelins, and dihydrosphingomyelins, compared to unexposed HFD-fed mice (Fig. 4E–L). Nevertheless, the total sphingomyelin level was reduced to a significantly lower level than that observed in unexposed CHOW-fed mice, the total ceramide level was reduced to the same level as that observed in unexposed CHOW-fed mice. Finally, in HFD-fed mice exposed to FB1, the dihydroceramide and dihydrosphingomyelin levels remained significantly higher than the levels observed in unexposed CHOW-fed mice.

Taken together, these results suggest that HFD-induced liver steatosis enhance FB1 effect on sphingolipid metabolism inhibiting more efficiently ceramide synthase. Surprisingly, under HFD-induced obesity FB1 seems to enhance sphingosine-kinase activity. Indeed, relative gene expression of SphK1 increases significantly under combined exposure of HFD and FB1 (Fig. S3A). Associated to this increase, both dihydro-sphingosine-1-phosphate and sphingosine-1-phosphate increase significantly in liver of HFD-fed mice exposed to FB1 compared to none exposed HFD-fed mice (Fig. S3B). Moreover, in HFD-induced obesity, FB1 also seems to prevent glycosphingolipid recycling decreasing the level of both glucosylceramides, lactosyl-ceramides, GM3 and GB3 (Fig. S3C–D).

3.5. Effect of FB1 on the hepatic metabolome

These severe metabolic effects on sphingolipids led us to explore the global metabolomic profile of the liver with an untargeted approach.

To investigate the effect of FB1 on hepatic metabolism, we performed ^1H NMR-based metabolic profiling on liver tissues. We generated O-PLS-DA plots derived from ^1H NMR spectra of aqueous hepatic extracts and compared the effects of FB1 exposure on the liver metabolic profile under either CHOW or HFD feeding. No significant effects of FB1 exposure on the profiles of CHOW-fed mice were observed (Fig. 5A). However, FB1 exposure left a clear, significant metabolic fingerprint in HFD-fed mice (Fig. 5B). The coefficient plot derived from the O-PLS-DA model for HFD-fed mice highlighted differences in the levels of particular metabolites associated with FB1-exposure (Fig. 5C). For example, FB1 exposure specifically impacted the ^1H NMR chemical shift signals of bile acids, glutamate, succinate, aspartate, dimethylamine, tauro-conjugated bile acids, choline, glycerophosphocholine (GPC), fumarate, tyrosine, and uridine.

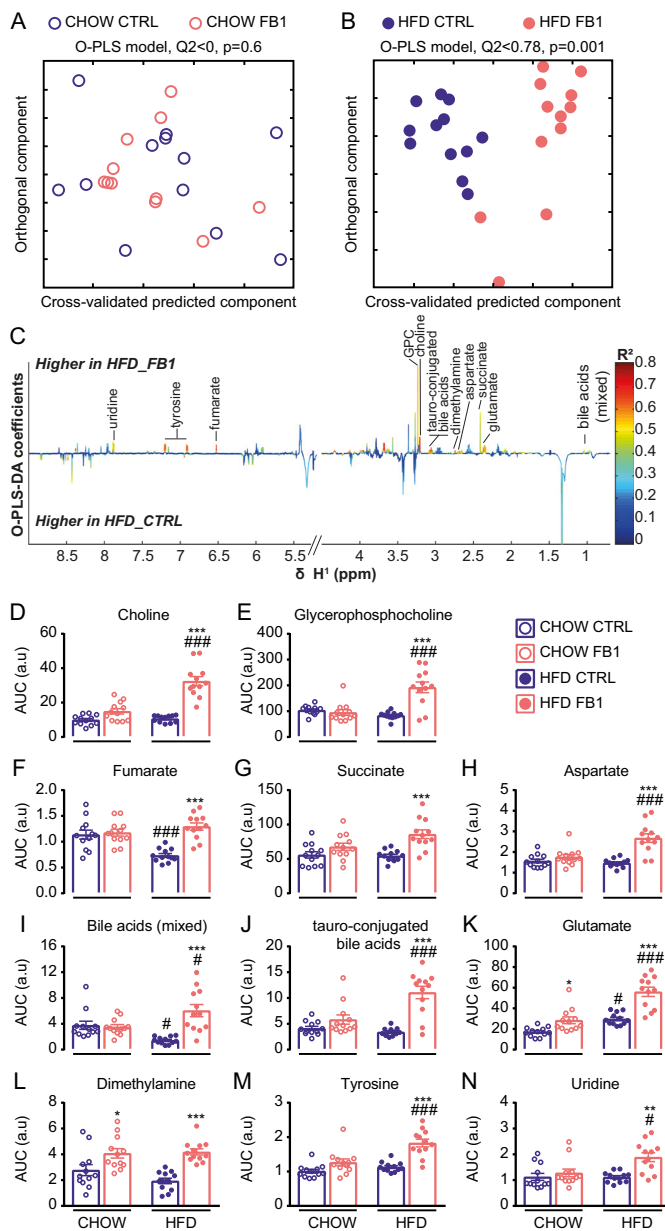


Fig. 5. FB1 effects on the metabolomic profile of the liver.

(A–B) O-PLS-DA score plots derived from the ^1H NMR metabolomic profiles of liver aqueous extracts from CHOW (A) or HFD (B)-fed mice. Each dot represents an animal. (C) Coefficient plots related to the O-PLS-DA models discriminating between HFD alone (HFD_CTRL) and HFD combined with FB1 exposure (HFD_FB1). Metabolites are color-coded according to their correlation coefficient. The direction of the metabolite peak indicates the group with which it was positively associated, as labeled on the diagram. (D–N) Areas under the curves for several discriminant metabolites selected using the previous O-PLS-DA model. Additional 2-way ANOVAs confirmed significant differences in metabolite levels ($n = 12/\text{group}$). Results are presented as the mean \pm SEM. # diet effect, * treatment effect. * or # p-value < 0.05, ** or ## p-value < 0.01, *** or ### p-value < 0.001; FB1: Fumonisin B1; CTRL: not exposed to FB1; O-PLS-DA: orthogonal projection on latent structure-discriminant analysis; GPC: glycerophosphocholine.

The areas under the curves of the ^1H NMR spectra were integrated for metabolites that were significantly correlated with the predictive component ($R^2 > 0.5$). Univariate statistics (1-way ANOVA + Sidak's post-tests) confirmed significant increases in the levels of metabolites involved in choline metabolism (choline and glycerophosphocholine); the tricarboxylic acid cycle (fumarate, succinate, aspartate, and glutamate); biliary acid

metabolism (mixed bile acids and tauro-conjugated bile acids); intestinal microbiota dysbiosis (dimethylamine and tyrosine), and uridine metabolism (Fig. 5D–N). These metabolic profile analyses confirmed that obesity induced by HFD feeding significantly influenced the effect of FB1 exposure on liver metabolism in vivo.

3.6. Effect of FB1 exposure on liver gene expression

We next performed an unbiased microarray analysis of liver gene expression to identify biological processes that were sensitive to FB1 exposure under both CHOW and HFD feeding. A principal component analysis (PCA) of the transcriptome showed a clear separation between CHOW-fed and HFD-fed groups (Fig. 6A). The separation observed along the second axis accounted for 13.6 % of the variance. Upon CHOW-fed, the unexposed and FB1 exposed groups overlapped. In contrast, the unexposed and FB1 exposed HFD-fed groups were clearly separated. The separation along the first axis accounted for 56.3 % of the variance.

Volcano plots of the FB1 effect upon CHOW-fed or HFD-fed mice confirmed the stronger genomic response to FB1 exposure with HFD feeding (Fig. 6B). Indeed, only 77 genes showed significantly modulated expression with FB1 exposure under the CHOW diet. In contrast, with the HFD, 9214 hepatic genes were differentially expressed in response to FB1 exposure (Fig. 6C).

We then performed hierarchical clustering to analyze the differentially expressed genes (those with adjusted p -values < 0.05), which corresponded to 11,920 probes (Fig. 6D). Along the horizontal axis, the blind clustering of profiles did not discriminate between FB1 exposed and unexposed mice under the CHOW diet. Conversely, HFD feeding induced marked clustering that discriminated clearly between unexposed mice and FB1 exposed mice. An analysis of the gene clustering revealed 6 major genetic groups along the vertical axis of the heatmap (Fig. 6D). Of these, four clusters were related to genes with similar expression levels in FB1-exposed mice under the CHOW diet but differentially expressed genes in FB1-exposed mice under HFD diet.

Expression of genes from clusters 1 and 2 was reduced upon FB1 exposure in HFD-fed mice. These genes were related to energy metabolism. In the first cluster, 668 genes showed an important increase in mRNA expression under the HFD compared to the CHOW diet. However, when the HFD group was exposed to FB1, mRNA expression was similar to the levels observed under the CHOW diet, with or without exposure to FB1. Moreover, the gene ontology enrichment analysis of this set of genes (Fig. 6E) revealed that the biological processes most significantly associated with this cluster were related to fatty acid beta-oxidation, very long-chain fatty acid metabolism, and the tricarboxylic acid cycle. Furthermore, characterization of the most significantly affected genes in cluster 1 (Fig. 6E) showed that, under HFD feeding, FB1 exposure essentially limited increases in the expression of genes involved in triglyceride storage, such as *Cidea*, *Fitm1*, *Plin4*, *Vldlr*, and *Elovl5*. In contrast, the 693 genes in cluster 2 showed an important reduction in mRNA expression under HFD feeding with FB1 exposure, compared to the CHOW-fed, unexposed group. Moreover, under HFD-feeding alone, mRNA expression was similar to the levels observed under the CHOW diet, with or without FB1 exposure. Similar to cluster 1, the gene ontology enrichment analysis of this set of genes (Fig. 6E) revealed that the biological processes most significantly associated with cluster 2 were: triglyceride metabolism, the tricarboxylic acid cycle, very long-chain fatty acid metabolism, carbohydrate catabolism, and steroid biosynthesis. Furthermore, characterization of the most significantly affected genes in cluster 2 (Fig. 6E) showed that, under HFD feeding, FB1 exposure reduced expression of genes involved in fatty acid metabolism, such as: *Elovl3* (involved in very long-chain fatty acid elongation from C18:0 to provide precursors for sphingolipid synthesis); *Acacb* and *Pdk1* (involved in fatty acid uptake and oxidation in mitochondria); and *Thrsp* (involved in lipid storage).

Clusters 4 and 5 included genes involved in cell cycle metabolism and organization. Indeed, the expression levels of the 1782 genes in cluster 4 were slightly decreased under the HFD, compared to the CHOW diet. However, a moderate increase in mRNA expression was observed with the HFD

and FB1 exposure, compared to the CHOW diet with FB1 exposure. Moreover, the gene ontology enrichment analysis (Fig. 6E) revealed that the biological processes most significantly associated with cluster 4 were translation, chromatin organization, and RNA splicing. Furthermore, characterization of the most significantly affected genes in cluster 4 (Fig. 6E) showed that, under HFD feeding, FB1 exposure reversed and slightly increased the expression of genes involved in cell proliferation (*Tgm1*, *Eppk1*) and cell junction organization (*Marveld2*, *Cdh1*). In cluster 5, the expression of 5189 genes significantly increased with the HFD and even more upon FB1 exposure, compared to the CHOW groups, without or with FB1 exposure. This effect indicated synergy between FB1 exposure and the HFD. The gene ontology enrichment analysis (Fig. 6E) revealed that the biological processes most significantly associated with cluster 5 were the mitotic cell cycle, extracellular matrix organization, RNA splicing, DNA repair, immune system processes, chromatin organization, and cell death. Furthermore, characterization of the most significantly affected genes in cluster 5 (Fig. 6E) showed that, under HFD feeding, FB1 exposure significantly amplified the expression of genes involved in cell cycle regulation (*Plk1*, *Prc1*, *Ube2c*, *Cdc20*, *Ccnb1*, *Cenpf*, *Cenpe*) and cytoskeleton organization (*Ckap2*, *Kif20a*, *Nusap1*, *Anln*).

At last, clusters 3 and 6 exhibited significant modulations with diet, independent of FB1 exposure. Indeed, in cluster 3, the expression levels of 889 genes associated with steroid biosynthesis or triglyceride metabolism decreased significantly under HFD feeding. In contrast, in cluster 6, the expression levels of 2699 genes associated with Golgi vesicle transport increased under the HFD.

4. Discussion

Environmental exposure to natural toxicants or chemical residues, alone or in mixtures, are frequently associated with the risk of chronic metabolic diseases (Grün and Blumberg, 2006). Moreover, the increasing prevalence of obesity (Estes et al., 2018), increases the risk of various diseases, including liver injuries. Several studies previously reported that toxicants, like triclosan (Yueh et al., 2020), 2,3,7,8-tetrachlorodibenzo-p-dioxin (Duval et al., 2017), chlorpyrifos (Wang et al., 2021), or methyl tert-butyl ether (Tang et al., 2019) contributed to the progression of obesity-associated liver steatosis. Those findings led us to hypothesize that environmental toxins may differentially impact liver homeostasis, depending on the presence of obesity. Among the natural food contaminants, some of the most prevalent and harmful mycotoxins are known to induce liver toxicity, such as aflatoxin B1 (Fan et al., 2021; Hua et al., 2021; Torres et al., 2020), T-2 toxin (Janik et al., 2021), deoxynivalenol (Hasuda et al., 2022), ochratoxin A (Tao et al., 2018), zearalenone (Wang et al., 2019), and FB1 (Wangia-Dixon and Nishimwe, 2021).

It is well-established that FB1 affects the gut-liver axis and liver metabolism (Terciolo et al., 2019; Régnier et al., 2017). Indeed, previous literature has described that exposure to oral FB1 disturbs extracellular matrix organization, immune response processes, and lipid homeostasis in both the intestine and liver (Devriendt et al., 2009; Dopavogui et al., 2022). Therefore, we tested the toxic effects of FB1 exposure in mice with diet-induced obesity. First, as expected, we showed that HFD feeding induced obesity, increased fasting glycemia, and hepatic steatosis (Régnier et al., 2020; Tamura and Shimomura, 2005). Second, we confirmed the known effect of FB1 exposure on sphingolipid homeostasis, which resulted in an increase in the Sa/So ratio (Régnier et al., 2019a, b; Loiseau et al., 2015). Although under HFD diet these effects are marked, the choice of murine species (C57BL6J), gender (male) and dose of FB1 revealed a very limited effect of this toxin at the hepatic level under standard diet: only a small increase of Sa/So ratio with an increase of both types of sphingoid bases, a single decrease of ceramide (d18:1; C16:0) and of an accumulation of d18:0 saturated dihydroceramides from C18:0 to C24:0. Similarly under CHOW diet only 77 genes were significantly modulated compared to over 9214 genes under the HFD diet. Then, we observed that HFD-induced obesity followed by 3 weeks of co-exposure to an HFD and FB1 resulted in gut dysbiosis, increased plasma FB1 levels, and reductions in body weight, liver

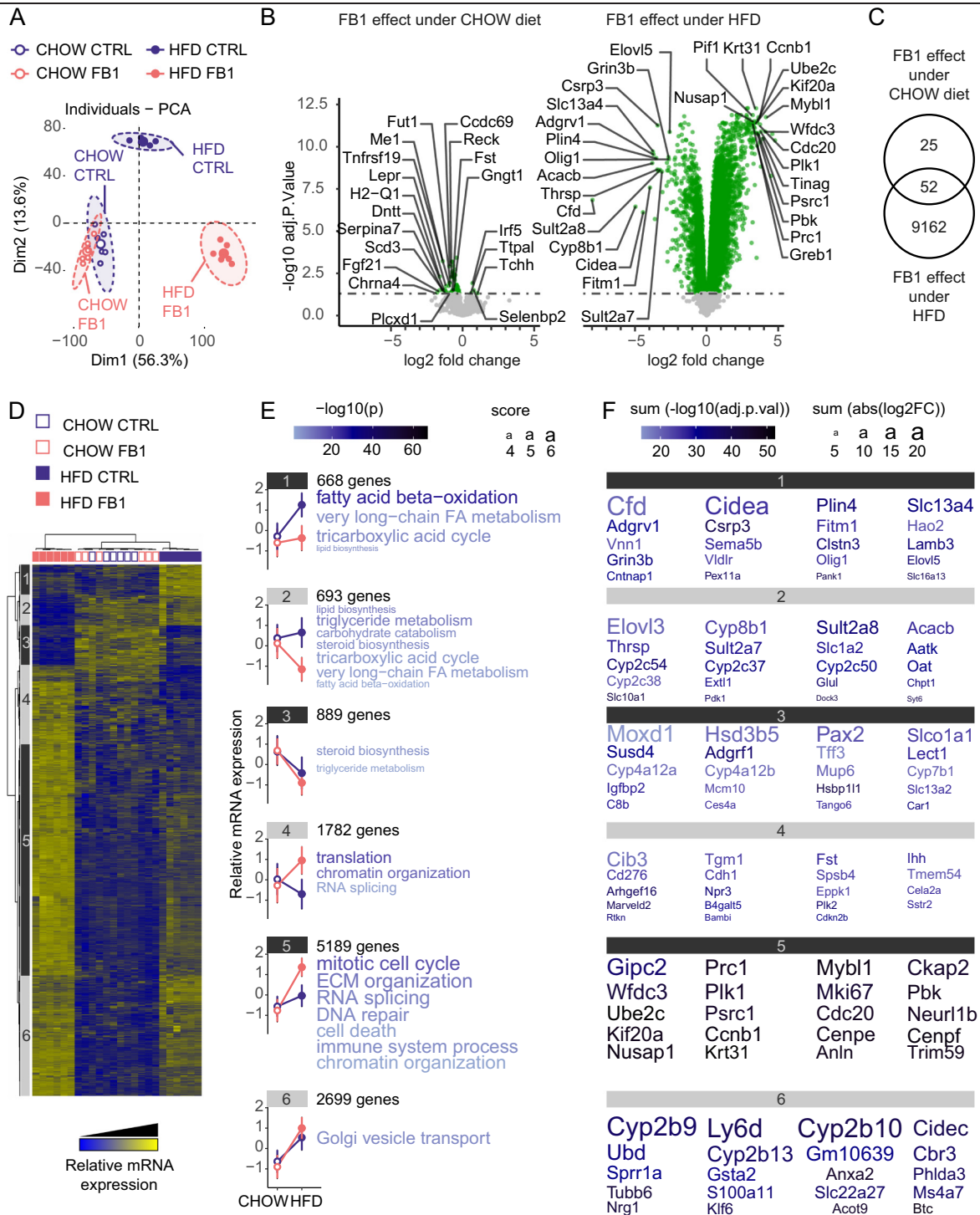


Fig. 6. FB1 effects on liver gene expression.

Gene expression profiles were analyzed in liver samples with Agilent microarrays ($n = 6/\text{group}$). (A) Principal component analysis (PCA) score plots of whole-liver transcriptome datasets ($n = 6/\text{group}$). Each dot represents an observation (animal), projected onto first (horizontal axis) and second (vertical axis) PCA variables. (B) Volcano plot shows FB1 effects on gene expression under a CHOW diet (left panel) or an HFD (right panel). Each gene expression level is shown in terms of the $-\log_{10}$ p-value, for comparisons between the FB1 exposed group and the unexposed (CTRL) group for each diet. The $-\log_{10}$ p-values are plotted as a function of the associated \log_2 -fold change, or formally, $\log_2(\text{FB1})-\log_2(\text{CTRL})$. The green points have p-values < 0.05 . Gene names are highlighted for the most highly regulated genes, according to a score based on the adjusted p-value $\times \log_2(\text{FC})$. (C) Venn diagram represents the number of genes significantly regulated by FB1 exposure for each diet. (D) Heatmap represents data from microarray experiments. The significantly differentially expressed genes (adjusted p-values < 0.05) were selected, and they corresponded to 11,920 probes. The color gradient indicates the scaled values of gene expression. Hierarchical clustering identified six gene clusters (indicated on the left). (E) Mean expression profiles for the six gene clusters. Graphs represent the means of the scaled gene expression values. Error bars are standard deviations. The most significantly enriched biological processes identified with the Metascape gene ontology algorithm are shown at the right of each profile. Briefly, hypergeometric tests were performed for each category in each cluster. The size of the font is related to a score based on the log base 2 number of genes enriched, and the color gradients of the characters represent the $-\log$ base 10 value of the probability of the test for $P[X > x]$. (F) Representation of the top 20 genes in each cluster that showed the largest differences in expression. The color of each character string is related to the sum of the $-\log_{10}(\text{adjusted p-value})$, and the size of each character string is related to the sum of the absolute $\log_2\text{FC}$ values for all the comparisons made for each gene.

weight, fasting blood glucose, and triglyceride levels. However, several plasma markers of liver injury (ALT, AST, ALP, and bilirubin) were significantly increased, which indicated severe hepatitis. Finally, unbiased analyses of the liver metabolome and transcriptome produced results consistent with the notion that FB1 exposure had a potent effect on liver metabolism, which is additive to the effects of diet-induced obesity.

Several lines of evidence have suggested that environmental toxicants may influence obesity and NAFLD (Rajak *et al.*, 2021). However, most pre-clinical studies supporting this hypothesis were co-exposure studies. In contrast, the present study took an original approach by exposing mice to FB1 after they became obese and hyperglycemic on the HFD. We monitored body weight and water intake to ensure that chow-fed and HFD-fed mice were exposed to a similar dose of FB1 relative to body weight. Thus, with similar FB1 dosing, normal and obese mice showed different systemic and hepatic responses to FB1. However, the plasma FB1 levels were different in CHOW and HFD groups. This result might be due to either increased FB1 absorption or reduced FB1 clearance in the HFD-fed mice.

This study had some limitations. First, our study design did not allow us to determine the mechanism by which HFD exposure induces the increase in circulating plasma level of FB1. The HFD might have changed the gut physiology, altered the microbiota composition and/or activity (Rohr *et al.*, 2020; Mouries *et al.*, 2019), or suppressed FB1 detoxication; indeed, both obesity and hepatic steatosis are known to hamper detoxification processes in the gut and liver (Cobbina and Akhlaghi, 2017; Sharpton *et al.*, 2019). Another limitation of the study was that we administered a high dose of FB1, which was hundred times above the BMDL₁₀ of 0.1 mg/kg bw per day calculated by the CONTAM Panel from EFSA and derived for induction of megalocytic hepatocytes in specific p53[±] mice (Bondy *et al.*, 2012; Knutsen *et al.*, 2018a). Thus, one might question the potential relevance of the findings to animal and human populations (Terciolo *et al.*, 2019). However, rodents are known to be particularly resistant to FB1 toxicity; indeed, in our study very few biological markers have been modulated in rodents under a regular CHOW diet. Only 77 genes were significantly modulated. Moreover, whereas usually FB1 exposure induces a strong decrease in all ceramide and dihydroceramide species and an increase in the Sa/So ratio due to Sa accumulation and So depletion, here, within the FB1 dose studied, we observed only earlier effects of FB1 with a small increase in the Sa/So ratio with an increase in both types of sphingoid bases, a single decrease in ceramides (d18: 1; C16:0) and an accumulation of saturated dihydroceramides (d18:0) from C18:0 to C24:0. Nevertheless, the altered effects of HFD feeding and FB1 exposure observed in this study provided further evidence that obesity could weaken the host's ability to cope with food toxins, and revealed novel insights on the hepatic toxicity of FB1.

In obesity, the liver is exposed to increase in both endotoxin levels and metabolic stress. Both these factors promote NAFLD, which ranges in severity, from steatosis to steatohepatitis, cirrhosis, and cancer (Ferro *et al.*, 2020; Todoric *et al.*, 2020; Loo *et al.*, 2017; Kübeck *et al.*, 2016). Based on our histological analyses and our targeted assays on liver composition and function, we concluded that FB1 reduced the steatosis and neutral lipid deposition induced by HFD feeding. These effects were associated with reductions in body weight and hyperglycemia, which suggested that FB1 could reduce obesity and diabetes, which in turn, might have contributed to reducing hepatic lipid accumulation (Meikle and Summers, 2017; Holland and Summers, 2008). Our monitoring of food intake showed that whereas a lack of significant changes in food intake only applies to CHOW mice; a significant reduction was seen with HFD mice, both HFD alone and HFD + FB1. Nevertheless, considering the monitoring of calory intake, only a significant increase of calory intake has been shown for the HFD alone fed. This result suggested that FB1 affected calory absorption and/or expenditure. However, this hypothesis warrants future study, because it is beyond the direct effects of FB1 on hepatic homeostasis. Although FB1 exposure reduced steatosis in HFD-fed mice, it also significantly induced liver inflammation, damage, and dysfunction. Indeed, FB1-induced hepatitis was much more severe in HFD-fed mice than in CHOW-fed mice, and it was associated with a massive shift in liver metabolism and gene expression.

It remains unclear whether all of these HFD-exacerbated signs of FB1 toxicity were related to FB1 inhibition of sphingolipid synthesis or whether it involved multiple organ cross-talk between gut, liver and adipose tissues. In mice fed a standard diet and exposed to FB1, inhibition of ceramide synthase activity leads to reduced dihydroceramide, ceramide, and sphingomyelin levels. Concurrently, the inhibition of de novo sphingolipid biosynthesis causes an accumulation of dihydrosphingosine and sphingosine, with no significant effect on S1P or dihydrosphingosine-1-phosphate. However, in HFD-fed mice exposed to FB1, the initial state of the sphingolipidome before FB1 exposure influences the results. HFD-fed mice display a general increase in sphingolipids content, including ceramides, sphingomyelins, dihydroceramides, glycosphingolipids, but also sphingosine, and dihydrosphingosine. S1P significantly decreases in HFD-fed mice. However, FB1 exposure increases S1P level in HFD-fed mice. Recent findings showed that S1P plays an antidiabetic role by counteracting excessive inflammation and maintaining metabolic homeostasis (Chakrabarty *et al.*, 2022). Therefore, the effect of FB1 on S1P level in HFD fed mice may contribute to some of the metabolic effects of FB1 observed upon HFD feeding.

As expected, FB1 exposure in HFD-induced obese mice results in a decrease in dihydroceramides, ceramides, and sphingomyelins, and an accumulation of sphinganine. More surprisingly, FB1 causes a decrease in hepatic sphingosine and glycosphingolipid content and an accumulation of S1P and dihydrosphingosine-1-phosphate. These results suggest that FB1 exacerbates sphingoid base phosphorylation and significantly disrupts the sphingolipid salvage pathway in HFD-induced obese mice, potentially by disrupting the endolysosomal trafficking pathway. Sphingolipids, such as ceramides, are bioactive lipids that drive the progression of steatosis (Hannun and Obeid, 2018; Choi and Snider, 2015; Xia *et al.*, 2015). Indeed, several studies have identified correlations between dihydroceramides and different measures of NAFLD in humans (Ooi *et al.*, 2021; Vvedenskaya *et al.*, 2021). Additionally, various preclinical studies in rodents have demonstrated that ceramides and dihydroceramides are necessary for NAFLD development (Poss and Summers, 2020; Chaurasia *et al.*, 2016; Régnier *et al.*, 2019a, b). Therefore, the effects of FB1 that we observed on steatosis were consistent with an inhibition of the steatogenic role of ceramides (Chaurasia *et al.*, 2019; Holland and Summers, 2008). Furthermore, the effects of FB1 on liver damage and inflammation were consistent with an inhibition of the well-known pro-inflammatory and pro-apoptotic effects of sphingolipid species respectively such as S1P, dihydrosphingosine-1-phosphate and sphingoid bases (Molino *et al.*, 2017; Riley *et al.*, 2001). Therefore, the pro-inflammatory effects of FB1 observed in HFD-fed mice might have occurred as an indirect consequence of altered ceramide homeostasis (Chen *et al.*, 2021).

5. Conclusion

To our knowledge, the present study was the first to assess the effects of diet-induced obesity on FB1 toxicity. This work established that, in the context of obesity, FB1 exposure exhibited enhanced gut dysbiosis, systemic and hepatotoxic effects. Although FB1 exposure in diet-induced obese mice led to significant reductions in body weight, glycemia, and hepatic lipid content, it also induced liver inflammation and increases in various markers of hepatotoxicity. Therefore, our findings suggest that diet-induced obesity may increase the sensitivity to environmental toxins.

Supplementary data to this article can be found online at <https://doi.org/10.1016/j.scitotenv.2023.164436>.

CRediT authorship contribution statement

Conceptualization: N.L., H.G. and I.P.O.; Formal analysis: L.D., M.R., A.P., Y.L., J.B.M., L.De., J.C., S.C., B.C., S.E.S. and N.L.; Investigation: L.D., M.R., Q.P., S.S., W.K., F.L., C.L., A.F., J.B.M., C.N., C.C., E.R.B., L.G.P., C.D., J.C., S.D.B., H.M.B., S.E.S., H.G. and N.L.; Writing - original draft preparation, L.D. and N.L.; Writing - review and editing, N.L., H.G. and I.P.O.; Visualization, A.P. and N.L.; Supervision, N.L. and I.P.O.;

Funding acquisition, N.L. and I.P.O. All authors have read and agreed to the published version of the manuscript.

Data availability

Data will be made available on request.

Declaration of competing interest

The authors declare no competing financial interests or personal relationships that could have influenced the study.

Acknowledgements

L.D. PhD was supported by the INRAE Animal Health department. This work was also supported by grants from the French National Research Agency (ANR) Fumolip (ANR-16-CE21-0003) and the Hepatomics FEDER program of Région Occitanie. We thank Prof Wentzel C. Gelderblom for generously providing the FB1 and for his interest and support in our project. B.C. laboratory is supported by a Starting Grant from the European Research Council (ERC) under the European Union's Horizon 2020 research and innovation program (grant agreement No. ERC-2018-StG- 804135), a Chaire d'Excellence from IdEx Université de Paris - ANR-18-IDEX-0001, an Innovator Award from the Kenneth Rainin Foundation, an ANR grant EMULBIONT ANR-21-CE15-0042-01 and the national program "Microbiote" from INSERM. We thank Anexplo (Genotoul, Toulouse) for their excellent work on plasma biochemistry. Neutral Lipids MS and NMR experiments were performed with instruments in the Metatoul-AXIOM platform. Sphingolipid MS analysis were performed with instruments in the RUBAM platform. The FB1 plasma levels were determined using an UPLC-MS/MS instrument part of the Ghent University MSsmall expertise centre for advanced mass spectrometry analysis of small organic molecules. We thank Elodie Rousseau-Bacqué and all members of the EZOP staff for their assistance in the animal facility. We are very grateful to Talal al Saati for histology analyses and review, and we thank all members of the US006/CREFRE staff at the histology facility and the GenomIC platforms (INSERM U1016, Paris, France) for their expertise.

References

- (EC) No 1126, 2007. Commission Regulation, 2007. Commission Regulation (EC) No 1126/2007.
- (EC) No 576, 2006. Commission Recommendation, 2006. Commission Recommendation (EC) No 576/2006.
- Barbacini, P., Casas, J., Torretta, E., Capitanio, D., Maccallini, G., Hirschler, V., Gelfi, C., 2019. Regulation of serum sphingolipids in Andean children born and living at high altitude (3775 m). *Int. J. Mol. Sci.* 20. <https://doi.org/10.3390/IJMS20112835>.
- Bolyen, E., Rideout, J.R., Dillon, M.R., Bokulich, N.A., Abnet, C.C., Al-Ghalith, G.A., Alexander, H., Alm, E.J., Arumugam, M., Asnicar, F., Bai, Y., Bisanz, J.E., Bittinger, K., Brejnrod, A., Brislawn, C.J., Brown, C.T., Callahan, B.J., Caraballo-Rodríguez, A.M., Chase, J., Cope, E.K., Da Silva, R., Diener, C., Dorrestein, P.C., Douglas, G.M., Durall, D.M., Duvallet, C., Edwardson, C.F., Ernst, M., Estaki, M., Fouquier, J., Gauglitz, J.M., Gibbons, S.M., Gibson, D.L., Gonzalez, A., Gorlick, K., Guo, J., Hillmann, B., Holmes, S., Holste, H., Huttenhower, C., Huttley, G.A., Janssen, S., Jarmusch, A.K., Jiang, L., Kaehler, B.D., Kang, K. Bin, Keefe, C.R., Keim, P., Kelley, S.T., Knights, D., Koester, I., Kosciolk, T., Krets, J., Langille, M.G.I., Lee, J., Ley, R., Liu, Y.X., Loftfield, E., Lozupone, C., Maher, M., Marotz, C., Martin, B.D., McDonald, D., McIver, L.J., Melnik, A.V., Metcalf, J.L., Morgan, S.C., Morton, J.T., Naimey, A.T., Navas-Molina, J.A., Nothias, L.F., Orchanian, S.B., Pearson, T., Peoples, S.L., Petras, D., Preuss, M.L., Pruesse, E., Rasmussen, L.B., Rivers, A., Robeson, M.S., Rosenthal, P., Segata, N., Shaffer, M., Shiffer, A., Sinha, R., Song, S.J., Spear, J.R., Swafford, A.D., Thompson, L.R., Torres, P.J., Trinh, P., Tripathi, A., Turnbaugh, P.J., Ul-Hasan, S., van der Hoof, J.J.J., Vargas, F., Vázquez-Baeza, Y., Vogtmann, E., von Hippel, M., Walters, W., Wan, Y., Wang, M., Warren, J., Weber, K.C., Williamson, C.H.D., Willis, A.D., Xu, Z.Z., Zaneveld, J.R., Zhang, Y., Zhu, Q., Knight, R., Caporaso, J.G., 2019. Reproducible, interactive, scalable and extensible microbiome data science using QIIME 2. *Nat. Biotechnol.* 37, 852–857. <https://doi.org/10.1038/s41587-019-0209-9> (2019 378).
- Bondy, G., Mehta, R., Caldwell, D., Coady, L., Armstrong, C., Savard, M., Miller, J.D., Chomyshyn, E., Bronson, R., Zitomer, N., Riley, R.T., 2012. Effects of long term exposure to the mycotoxin fumonisin B1 in p53 heterozygous and p53 homozygous transgenic mice. *Food Chem. Toxicol.* 50, 3604–3613. <https://doi.org/10.1016/j.fct.2012.07.024>.
- Bouhet, S., Le Dorze, E., Peres, S., Fairbrother, J.M., Oswald, I.P., 2006. Mycotoxin fumonisin B1 selectively down-regulates the basal IL-8 expression in pig intestine: in vivo and

- in vitro studies. *Food Chem. Toxicol.* 44, 1768–1773. <https://doi.org/10.1016/J.FCT.2006.05.018>.
- Brozinick, J.T., Hawkins, E., Hoang Bui, H., Kuo, M.S., Tan, B., Kievit, P., Grove, K., 2013. Plasma sphingolipids are biomarkers of metabolic syndrome in non-human primates maintained on a Western-style diet. *Int. J. Obes.* 37, 1064–1070. <https://doi.org/10.1038/ijo.2012.191>.
- Callahan, B.J., McMurdie, P.J., Rosen, M.J., Han, A.W., Johnson, A.J.A., Holmes, S.P., 2016. DADA2: high-resolution sample inference from Illumina amplicon data. *Nat. Methods* 13, 581–583. <https://doi.org/10.1038/nmeth.3869> (2016 137).
- Cano, P.M., Puel, O., Oswald, I.P., 2016. Mycotoxins: fungal secondary metabolites with toxic properties. In: Misra, J., Tewari, J., Papp, T. (Eds.), *Fungi. Applications and management strategies. Progress in Mycological Research* 2016. CRC Press, pp. 318–371 (978-1-4987-2492-0. [hal-01607873](https://doi.org/10.1016/B978-1-4987-2492-0.ch16)).
- Chakrabarty, S., Bui, Q., Badeanlou, L., Hester, K., Chun, J., Ruf, W., Ciaraldi, T.P., Samad, F., 2022. S1P/S1PR3 signalling axis protects against obesity-induced metabolic dysfunction. *Adipocyte*. 11, 69–83. <https://doi.org/10.1080/21623945.2021.2021700>.
- Chassaing, B., Koren, O., Goodrich, J.K., Poole, A.C., Srinivasan, S., Ley, R.E., Gewirtz, A.T., 2015. Dietary emulsifiers impact the mouse gut microbiota promoting colitis and metabolic syndrome. *Nature* 519, 92–96. <https://doi.org/10.1038/NATURE14232> (2015 5197541).
- Chaurasia, B., Kaddai, V.A., Lancaster, G.I., Henstridge, D.C., Sriram, S., Galam, D.L.A., Gopalan, V., Prakash, K.N.B., Velan, S.S., Bulchand, S., Tsong, T.J., Wang, M., Siddique, M.M., Yuguang, G., Sigmundsson, K., Mellet, N.A., Weir, J.M., Meikle, P.J., Bin, M., Yassin, M.S., Shabbir, A., Shayman, J.A., Hirabayashi, Y., Shioh, S.A.T.E., Sugii, S., Summers, S.A., 2016. Adipocyte ceramides regulate subcutaneous adipose browning, inflammation, and metabolism. *Cell Metab.* 24. <https://doi.org/10.1016/j.cmet.2016.10.002>.
- Chaurasia, B., Tippetts, T.S., Monibas, R.M., Liu, J., Li, Y., Wang, Liping, Wilkerson, J.L., Rufus Sweeney, C., Pereira, R.F., Sumida, D.H., Alan Maschek, J., Cox, J.E., Kaddai, V., Lancaster, G.I., Siddique, M.M., Poss, A., Pearson, M., Satapati, S., Zhou, H., McLaren, D.G., Previs, S.F., Chen, Y., Qian, Y., Petrov, A., Wu, M., Shen, X., Yao, J., Nunes, C.N., Howard, A.D., Wang, Liangsu, Erion, M.D., Rutter, J., Holland, W.L., Kelley, D.E., Summers, S.A., 2019. Targeting a ceramide double bond improves insulin resistance and hepatic steatosis. *Science* 365, 386–392. <https://doi.org/10.1126/SCIENCE.AAV3722>.
- Chen, J., Wei, Z., Wang, Y., Long, M., Wu, W., Kuca, K., 2021. Fumonisin B₁: mechanisms of toxicity and biological detoxification progress in animals. *Food Chem. Toxicol.* 149, 111977. <https://doi.org/10.1016/j.fct.2021.111977> Mar; Epub 2021 Jan 9. PMID: 33428988.
- Choi, S., Snider, A.J., 2015. Sphingolipids in high fat diet and obesity-related diseases. *Mediat. Inflamm.* 2015. <https://doi.org/10.1155/2015/520618>.
- Cirulli, E.T., Guo, L., Leon Swisher, C., Shah, N., Huang, L., Napier, L.A., Kirkness, E.F., Spector, T.D., Caskey, C.T., Thorens, B., Venter, J.C., Telenti, A., 2019. Profound perturbation of the metabolome in obesity is associated with health risk. *Cell Metab.* 29, 488–500.e2. <https://doi.org/10.1016/j.cmet.2018.09.022>.
- Cloarec, O., Dumas, M.E., Craig, A., Barton, R.H., Trygg, J., Hudson, J., Blancher, C., Gauguier, D., Linder, J.C., Holmes, E., Nicholson, J., 2005. Statistical total correlation spectroscopy: an exploratory approach for latent biomarker identification from metabolic 1H NMR data sets. *Anal. Chem.* 77, 1282–1289. <https://doi.org/10.1021/AC048630X>.
- Cobbina, E., Akhlaghi, F., 2017. Non-alcoholic fatty liver disease (NAFLD) - pathogenesis, classification, and effect on drug metabolizing enzymes and transporters. *Drug Metab. Rev.* 49, 197–211. <https://doi.org/10.1080/03602532.2017.1293683>.
- Contos, M.J., Cales, W., Sterling, R.K., Luketic, V.A., Shiffman, M.L., Mills, A.S., Fisher, R.A., Ham, J., Sanyal, A.J., 2001. Development of nonalcoholic fatty liver disease after orthotopic liver transplantation for cryptogenic cirrhosis. *Liver Transpl.* 7, 363–373. <https://doi.org/10.1053/jlts.2001.23011>.
- De Baere, S., Croubels, S., Novak, B., Bichl, G., Antonissen, G., 2018. Development and validation of a UPLC-MS/MS and UPLC-HR-MS method for the determination of fumonisin B1 and its hydrolysed metabolites and fumonisin B2 in broiler chicken plasma. *Toxins (Basel)* 10. <https://doi.org/10.3390/TOXINS10020062>.
- Devriendt, B., Gallois, M., Verdonck, F., Wache, Y., Bimczok, D., Oswald, I.P., Goddeeris, B.M., Cox, E., 2009. The food contaminant fumonisin B(1) reduces the maturation of porcine CD11R1(+) intestinal antigen presenting cells and antigen-specific immune responses, leading to a prolonged intestinal ETEC infection. *Vet. Res.* 40, 40. <https://doi.org/10.1051/vetres/2009023>.
- Dietlerle, F., Ross, A., Schlotterbeck, G., Senn, H., 2006. Probabilistic quotient normalization as robust method to account for dilution of complex biological mixtures. Application in 1H NMR metabolomics. *Anal. Chem.* 78, 4281–4290. <https://doi.org/10.1021/AC051632C>.
- Dopavogui, L., Polizzi, A., Fougerat, A., Gourbeyre, P., Terciolo, C., Klement, W., Pinton, P., Laffite, J., Cossalter, A.M., Bailly, J.D., Puel, O., Lippi, Y., Naylies, C., Guillou, H., Oswald, I.P., Loiseau, N., 2022. Tissue genomic responses to oral FB1 exposure in pigs. *Toxins (Basel)* 14, 83. <https://doi.org/10.3390/toxins14020083>.
- Duval, C., Teixeira-Clerc, F., Leblanc, A.F., Touch, S., Emond, C., Guerre-Millo, M., Lotersztajn, S., Barouki, R., Aggerbeck, M., Coumoul, X., 2017. Chronic exposure to low doses of dioxin promotes liver fibrosis development in the C57BL/6J diet-induced obesity mouse model. *Environ. Health Perspect.* 125, 428–436. <https://doi.org/10.1289/EHP316>.
- Estes, C., Razavi, H., Loomba, R., Younossi, Z., Sanyal, A.J., 2018. Modeling the epidemic of nonalcoholic fatty liver disease demonstrates an exponential increase in burden of disease. *Hepatology* 67, 123–133. <https://doi.org/10.1002/hep.29466>.
- Fan, T., Xie, Y., Ma, W., 2021. Research progress on the protection and detoxification of phytochemicals against aflatoxin B1-induced liver toxicity. *Toxicol* 195, 58–68. <https://doi.org/10.1016/J.TOXICON.2021.03.007>.
- Ferro, D., Baratta, F., Pastori, D., Cocomello, N., Colantoni, A., Angelico, F., Del Ben, M., 2020. New insights into the pathogenesis of non-alcoholic fatty liver disease: gut-derived lipopolysaccharides and oxidative stress. *Nutrients* 12, 1–14. <https://doi.org/10.3390/NU12092762>.

- Grenier, B., Bracarense, A.P., Schwartz, H.E., Trumel, C., Cossalter, A.M., Schatzmayr, G., Kolf-Clauw, M., Moll, W.D., Oswald, I.P., 2012. The low intestinal and hepatic toxicity of hydrolyzed fumonisin B₁ correlates with its inability to alter the metabolism of sphingolipids. *Biochem. Pharmacol.* 83, 1465–1473. <https://doi.org/10.1016/j.bcp.2012.02.007>.
- Grün, F., Blumberg, B., 2006. Environmental obesogens: organotins and endocrine disruption via nuclear receptor signaling. *Endocrinology* 147, s50–s55. <https://doi.org/10.1210/EN.2005-1129>.
- Hage Hassan, R., Bourron, O., Hajdúch, E., 2014. Defect of insulin signal in peripheral tissues: important role of ceramide. *World J. Diabetes* 5, 244–257. <https://doi.org/10.4239/wjdv5.i3.244>.
- Hajdúch, E., Lachkar, F., Ferré, P., Fougelle, F., 2021. Roles of ceramides in non-alcoholic fatty liver disease. *J. Clin. Med.* 10, 792. <https://doi.org/10.3390/jcm10040792>.
- Halloy, D.J., Gustin, P.G., Bouhet, S., Oswald, I.P., 2005. Oral exposure to culture material extract containing fumonisins predisposes swine to the development of pneumonitis caused by *Pasteurella multocida*. *Toxicology* 213, 34–44. <https://doi.org/10.1016/J.TOX.2005.05.012>.
- Hannun, Y.A., Obeid, L.M., 2018. Sphingolipids and their metabolism in physiology and disease. *Nat. Rev. Mol. Cell Biol.* 19, 175–191. <https://doi.org/10.1038/NRM.2017.107>.
- Hasuda, A.L., Person, E., Khoshal, A.K., Bruel, S., Puel, S., Oswald, I.P., Bracarense, A.P.F.R.L., Pinton, P., 2022. Deoxyvinalein induces apoptosis and inflammation in the liver: analysis using precision-cut liver slices. *Food Chem. Toxicol.* 163, 112930. <https://doi.org/10.1016/J.FCT.2022.112930>.
- Holland, W.L., Summers, S.A., 2008. Sphingolipids, insulin resistance, and metabolic disease: new insights from in vivo manipulation of sphingolipid metabolism. *Endocr. Rev.* 29, 381–402. <https://doi.org/10.1210/er.2007-0025>.
- Holland, W.L., Brozinick, J.T., Wang, L.P., Hawkins, E.D., Sargent, K.M., Liu, Y., Narra, K., Hoehn, K.L., Knotts, T.A., Siesky, A., Nelson, D.H., Karathanasis, S.K., Fontenot, G.K., Birnbaum, M.J., Summers, S.A., 2007. Inhibition of ceramide synthesis ameliorates glucocorticoid-, saturated-fat-, and obesity-induced insulin resistance. *Cell Metab.* 5, 167–179. <https://doi.org/10.1016/j.cmet.2007.01.002>.
- Hua, Z., Liu, R., Chen, Y., Liu, G., Li, C., Song, Y., Cao, Z., Li, Wen, Li, Weifeng, Lu, C., Liu, Y., 2021. Contamination of aflatoxins induces severe hepatotoxicity through multiple mechanisms. *Front. Pharmacol.* 11. <https://doi.org/10.3389/fphar.2020.605823>.
- Janik, E., Niemcewicz, M., Podogrocki, M., Ceremuga, M., Stela, M., Bijak, M., 2021. T-2 toxin — the most toxic trichothecene mycotoxin: metabolism, toxicity, and decontamination strategies. *Mol. 26*, 6868. <https://doi.org/10.3390/MOLECULES26226868> (2021, Vol. 26, Page 6868).
- Knutsen, H.K., Barregård, L., Bignami, M., Brüschweiler, B., Ceccatelli, S., Cottrill, B., Dinovi, M., Edler, L., Grasl-Kraupp, B., Hogstrand, C., Hoogenboom, L. (Ron), Nebbia, C.S., Petersen, A., Rose, M., Roudot, A., Schwerdtle, T., Vlemminck, C., Vollmer, G., Wallace, H., Dall'Asta, C., Gutleb, A.C., Humpf, H., Galli, C., Metzler, M., Oswald, I.P., Parent-Massin, D., Binaglia, M., Steinkellner, H., Alexander, J., Alexander, J., 2018a. Appropriateness to set a group health-based guidance value for fumonisins and their modified forms. *EFSA J.* 16. <https://doi.org/10.2903/j.efsfa.2018.5172>.
- Knutsen, H.K., Alexander, J., Barregård, L., Bignami, M., Brüschweiler, B., Ceccatelli, S., Cottrill, B., Dinovi, M., Edler, L., Grasl-Kraupp, B., Hogstrand, C., Hoogenboom, L. (Ron), Nebbia, C.S., Petersen, A., Rose, M., Roudot, A.C., Schwerdtle, T., Vlemminck, C., Vollmer, G., Wallace, H., Dall'Asta, C., Eriksen, G.S., Taranu, I., Altieri, A., Roldán-Torres, R., Oswald, I.P., 2018b. Risks for animal health related to the presence of fumonisins, their modified forms and hidden forms in feed. *EFSA J.* 16. <https://doi.org/10.2903/j.efsfa.2018.5242>.
- Kübeck, R., Bonet-Ripoll, C., Hoffmann, C., Walker, A., Müller, V.M., Schüppel, V.L., Lagkouvardos, I., Scholz, B., Engel, K.H., Daniel, H., Schmitt-Kopplin, P., Haller, D., Clavel, T., Klingenspor, M., 2016. Dietary fat and gut microbiota interactions determine diet-induced obesity in mice. *Mol. Metab.* 5, 1162–1174. <https://doi.org/10.1016/J.MOLMET.2016.10.001>.
- Loiseau, N., Debrauwer, L., Sambou, T., Bouhet, S., Miller, J.D., Martin, P.G., Viadère, J.L., Pinton, P., Puel, O., Pineau, T., Tulliez, J., Galtier, P., Oswald, I.P., 2007. Fumonisin B1 exposure and its selective effect on porcine jejunal segment: sphingolipids, glycolipids and trans-epithelial passage disturbance. *Biochem. Pharmacol.* 74, 144–152. <https://doi.org/10.1016/j.bcp.2007.03.031>.
- Loiseau, N., Polizzi, A., Dupuy, A., Therville, N., Rakotonirainy, M., Loy, J., Viadère, J.L., Cossalter, A.M., Bailly, J.D., Puel, O., Kolf-Clauw, M., Bertrand-Michel, J., Levade, T., Guillou, H., Oswald, I.P., 2015. New insights into the organ-specific adverse effects of fumonisin B1: comparison between lung and liver. *Arch. Toxicol.* 89, 1619–1629. <https://doi.org/10.1007/s00204-014-1323-6>.
- Longato, L., Tong, M., Wands, J.R., de la Monte, S.M., 2012. High fat diet induced hepatic steatosis and insulin resistance: role of dysregulated ceramide metabolism. *Hepatology*. Res. 42, 412–427. <https://doi.org/10.1111/j.1872-034X.2011.00934.x>.
- Loo, T.M., Kamachi, F., Watanabe, Y., Yoshimoto, S., Kanda, H., Arai, Y., Nakajima-Takagi, Y., Iwama, A., Koga, T., Sugimoto, Y., Ozawa, T., Nakamura, M., Kumagai, M., Watashi, K., Taketo, M.M., Aoki, T., Narumiya, S., Oshima, M., Arita, M., Hara, E., Ohtani, N., 2017. Gut microbiota promotes obesity-associated liver cancer through PGE 2-mediated suppression of antitumor immunity. *Cancer Discov.* 7, 522–538. <https://doi.org/10.1158/2159-8290.CD-16-0932>.
- Luukkonen, P.K., Zhou, Y., Sädevirta, S., Leivonen, M., Arola, J., Orešič, M., Hyötyläinen, T., Yki-Järvinen, H., 2016. Hepatic ceramides dissociate steatosis and insulin resistance in patients with non-alcoholic fatty liver disease. *J. Hepatol.* 64, 1167–1175. <https://doi.org/10.1016/j.jhep.2016.01.002>.
- Meikle, P.J., Summers, S.A., 2017. Sphingolipids and phospholipids in insulin resistance and related metabolic disorders. *Nat. Rev. Endocrinol.* <https://doi.org/10.1038/nrendo.2016.169>.
- Molino, S., Tate, E., McKillop, W., Medin, J.A., 2017. Sphingolipid pathway enzymes modulate cell fate and immune responses. *Immunotherapy* 9, 1185–1198. <https://doi.org/10.2217/IMT-2017-0089>.
- Montandon, S.A., Som, E., Loizides-Mangold, U., de Vito, C., Dibner, C., Jornayvaz, F.R., 2019. Multi-technique comparison of atherogenic and MCD NASH models highlights changes in sphingolipid metabolism. *Sci. Rep.* 9, 16810. <https://doi.org/10.1038/s41598-019-53346-4>.
- Mouries, J., Brescia, P., Silvestri, A., Spadoni, I., Sorribas, M., Wiest, R., Mileti, E., Galbiati, M., Invernizzi, P., Adorini, L., Penna, G., Rescigno, M., 2019. Microbiota-driven gut vascular barrier disruption is a prerequisite for non-alcoholic steatohepatitis development. *J. Hepatol.* 71, 1216–1228. <https://doi.org/10.1016/J.JHEP.2019.08.005>.
- Nakanishi, T., Fukui, H., Wang, X., Nishiumi, S., Yokota, H., Makizaki, Y., Tanaka, Y., Ohno, H., Tomita, T., Oshima, T., Miwa, H., 2021. Effect of a high-fat diet on the small-intestinal environment and mucosal integrity in the gut-liver axis. *Cells*. 10, 3168. <https://doi.org/10.3390/cells10113168>.
- Nnadi, N.E., Carter, D.A., 2021. Climate change and the emergence of fungal pathogens. *PLoS Pathog.* 17 (4), e1009503. <https://doi.org/10.1371/journal.ppat.1009503> Apr 29; PMID: 33914854; PMCID: PMC8084208.
- Ooi, G.J., Meikle, P.J., Huynh, K., Earnest, A., Roberts, S.K., Kemp, W., Parker, B.L., Brown, W., Burton, P., Watt, M.J., 2021. Hepatic lipidomic remodeling in severe obesity manifests with steatosis and does not evolve with non-alcoholic steatohepatitis. *J. Hepatol.* 75, 524–535. <https://doi.org/10.1016/j.jhep.2021.04.013>.
- Pillon, N.J., Loos, R.J.F., Marshall, S.M., Zierath, J.R., 2021. Metabolic consequences of obesity and type 2 diabetes: balancing genes and environment for personalized care. *Cell* 184, 1530–1544. <https://doi.org/10.1016/J.CELL.2021.02.012>.
- Poss, A.M., Summers, S.A., 2020. Too much of a good thing? An evolutionary theory to explain the role of ceramides in NAFLD. *Front. Endocrinol. (Lausanne)*, 11 <https://doi.org/10.3389/FENDO.2020.00505>.
- Raichur, S., Brunner, B., Bielohuby, M., Hansen, G., Pfeningner, A., Wang, B., Bruning, J.C., Larsen, P.J., Tennagels, N., 2019. The role of C16:0 ceramide in the development of obesity and type 2 diabetes: CerS6 inhibition as a novel therapeutic approach. *Mol. Metab.* 21, 36–50. <https://doi.org/10.1016/j.molmet.2018.12.008>.
- Rajak, S., Raza, S., Tewari, A., Sinha, R., 2021. Environmental toxicants and NAFLD: a neglected yet significant relationship. *Dig. Dis. Sci.* <https://doi.org/10.1007/S10620-021-07203-Y>.
- Régnier, M., Goubeyre, P., Pinton, P., Napper, S., Laffite, J., Cossalter, A.-M., Bailly, J.-D., Lippi, Y., Bertrand-Michel, J., Bracarense, A.P.F.R.L., Guillou, H., Loiseau, N., Oswald, I.P., 2017. Identification of signaling pathways targeted by the food contaminant FB1: transcriptome and kinome analysis of samples from pig liver and intestine. *Mol. Nutr. Food Res.* 61, 1700433. <https://doi.org/10.1002/mnfr.201700433>.
- Régnier, M., Polizzi, A., Guillou, H., Loiseau, N., 2019a. Sphingolipid metabolism in non-alcoholic fatty liver diseases. *Biochimie* 159, 9–22. <https://doi.org/10.1016/J.BIOCHIM.2018.07.021>.
- Régnier, M., Polizzi, A., Lukowicz, C., Smati, S., Lasserre, F., Lippi, Y., Naylies, C., Laffite, J., Bétoulières, C., Montagner, A., Duché, S., Goubeyre, P., Ellero-Simatos, S., Menard, S., Bertrand-Michel, J., Al Saati, T., Lobaccaro, J.M., Burger, H.M., Gelderblom, W.C., Guillou, H., Oswald, I.P., Loiseau, N., 2019b. The protective role of liver X receptor (LXR) during fumonisin B1-induced hepatotoxicity. *Arch. Toxicol.* 93, 505–517. <https://doi.org/10.1007/S00204-018-2345-2>.
- Régnier, M., Polizzi, A., Smati, S., Lukowicz, C., Fougerat, A., Lippi, Y., Fouché, E., Lasserre, F., Naylies, C., Bétoulières, C., Barquissau, V., Mouisel, E., Bertrand-Michel, J., Batut, A., Al Saati, T., Canlet, C., Tremblay-Franco, M., Ellero-Simatos, S., Langin, D., Postic, C., Wahli, W., Loiseau, N., Guillou, H., Montagner, A., 2020. Hepatocyte-specific deletion of Ppara promotes NAFLD in the context of obesity. *Sci. Rep.* 10, 1–15. <https://doi.org/10.1038/s41598-020-63579-3> (2020 101).
- Riley, R.T., An, N.H., Showker, J.L., Yoo, H.S., Norred, W.P., Chamberlain, W.J., Wang, E., Merrill, A.H., Motelin, G., Beasley, V.R., 1993. Alteration of tissue and serum sphinganine to sphingosine ratio: an early biomarker of exposure to fumonisin-containing feeds in pigs. *Toxicol. Appl. Pharmacol.* 118, 105–112. <https://doi.org/10.1006/taap.1993.1015>.
- Riley, R.T., Enongene, E., Voss, K.A., Norred, W.P., Meredith, F.I., Sharma, R.P., Spitsbergen, J., Williams, D.E., Carlson, D.B., Merrill Jr., A.H., 2001. Sphingolipid perturbations as mechanisms for fumonisin carcinogenesis. *Environ. Health Perspect.* 109 (Suppl. 2), 301–308. <https://doi.org/10.1289/ehp.01109s2301>.
- Ristic-Medic, D., Bajerska, J., Vucic, V., 2022. Crosstalk between dietary patterns, obesity and nonalcoholic fatty liver disease. *World J. Gastroenterol.* 28, 3314–3333. <https://doi.org/10.3748/wjg.v28.i27.3314>.
- Rohm, T.V., Meier, D.T., Olefsky, J.M., Donath, M.Y., 2022. Inflammation in obesity, diabetes, and related disorders. *Immunity* 55, 31–55. <https://doi.org/10.1016/J.IMMUNI.2021.12.013>.
- Rohr, M.W., Narasimhulu, C.A., Rudeski-Rohr, T.A., Parthasarathy, S., 2020. Negative effects of a high-fat diet on intestinal permeability: a review. *Adv. Nutr.* 11, 77–91. <https://doi.org/10.1093/ADVANCES/NMZ061>.
- Samad, F., Hester, K.D., Yang, G., Hannun, Y.A., Bielawski, J., 2006. Altered adipose and plasma sphingolipid metabolism in obesity: a potential mechanism for cardiovascular and metabolic risk. *Diabetes* 55, 2579–2587. <https://doi.org/10.2337/db06-0330>.
- Sharpton, S.R., Yong, G.J.M., Terrault, N.A., Lynch, S.V., 2019. Gut microbial metabolism and nonalcoholic fatty liver disease. *Hepatology*. Commun. 3, 29–43. <https://doi.org/10.1002/HEP4.1284>.
- Suez, J., Korem, T., Zeevi, D., Zilberman-Schapira, G., Thaiss, C.A., Maza, O., Israeli, D., Zmora, N., Gilad, S., Weinberger, A., Kuperman, Y., Harmelin, A., Kolodkin-Gal, I., Shapiro, H., Halpern, Z., Segal, E., Elinav, E., 2014. Artificial sweeteners induce glucose intolerance by altering the gut microbiota. *Nat* 514, 181–186. <https://doi.org/10.1038/NATURE13793> (2014 5147521).
- Sun, J., Fang, R., Wang, H., Xu, D.X., Yang, J., Huang, X., Cozzolino, D., Fang, M., Huang, Y., 2022. A review of environmental metabolism disrupting chemicals and effect biomarkers associating disease risks: where exposomics meets metabolomics. *Environ. Int.* 158. <https://doi.org/10.1016/J.ENVINT.2021.106941>.
- Tamura, S., Shimomura, I., 2005. Contribution of adipose tissue and de novo lipogenesis to nonalcoholic fatty liver disease. *J. Clin. Invest.* 115, 1139–1142. <https://doi.org/10.1172/JCI24930>.

- Tang, Y., Ren, Q., Wen, Q., Yu, C., Xie, X., Hu, Q., Du, Y., 2019. Effect of methyl tert-butyl ether on adipogenesis and glucose metabolism in vitro and in vivo. *J. Environ. Sci.* 85, 208–219. <https://doi.org/10.1016/J.JES.2019.06.015>.
- Tao, Y., Xie, S., Xu, F., Liu, A., Wang, Y., Chen, D., Pan, Y., Huang, L., Peng, D., Wang, X., Yuan, Z., 2018. Ochratoxin a: toxicity, oxidative stress and metabolism. *Food Chem. Toxicol.* 112, 320–331. <https://doi.org/10.1016/J.FCT.2018.01.002>.
- Terciolo, C., Bracarense, A.P., Souto, P.C.M.C., Cossalter, A.M., Dopavogui, L., Loiseau, N., Oliveira, C.A.F., Pinton, P., Oswald, I.P., 2019. Fumonisin at doses below EU regulatory limits induce histological alterations in piglets. *Toxins (Basel)* 11. <https://doi.org/10.3390/TOXINS11090548>.
- Todoric, J., Di Caro, G., Reibe, S., Henstridge, D.C., Green, C.R., Vrbanac, A., Ceteci, F., Conche, C., McNulty, R., Shalpour, S., Taniguchi, K., Meikle, P.J., Watrous, J.D., Moranchel, R., Najhawan, M., Jain, M., Liu, X., Kisseleva, T., Diaz-Meco, M.T., Moscat, J., Knight, R., Greten, F.R., Lau, L.F., Metallo, C.M., Febbraio, M.A., Karin, M., 2020. Fructose stimulated de novo lipogenesis is promoted by inflammation. *Nat. Metab.* 2, 1034–1045. <https://doi.org/10.1038/S42255-020-0261-2>.
- Torres, M.C.P., Bodini, G., Furnari, M., Marabotto, E., Zentilin, P., Giannini, E.G., 2020. Nuts and non-alcoholic fatty liver disease: are nuts safe for patients with fatty liver disease? *Nutr* 12, 3363. <https://doi.org/10.3390/NU12113363> (2020, Vol. 12, Page 3363).
- Veselkov, K.A., Lindon, J.C., Ebbels, T.M.D., Crockford, D., Volynkin, V.V., Holmes, E., Davies, D.B., Nicholson, J.K., 2009. Recursive segment-wise peak alignment of biological (1)h NMR spectra for improved metabolic biomarker recovery. *Anal. Chem.* 81, 56–66. <https://doi.org/10.1021/AC8011544>.
- Vvedenskaya, O., Rose, T.D., Knittelfelder, O., Palladini, A., Wodke, J.A.H., Schuhmann, K., Ackerman, J.M., Wang, Y., Has, C., Brosch, M., Thangapandi, V.R., Buch, S., Züllig, T., Hartler, J., Köfeler, H.C., Röcken, C., Coskun, Ü., Klipp, E., von Schoenfels, W., Gross, J., Schafmayer, C., Hampe, J., Pauling, J.K., Shevchenko, A., 2021. Nonalcoholic fatty liver disease stratification by liver lipidomics. *J. Lipid Res.* 62, 100104. <https://doi.org/10.1016/j.jlr.2021.100104>.
- Wang, E., Norred, W.P., Bacon, C.W., Riley, R.T., Merrill, A.H., 1991. Inhibition of sphingolipid biosynthesis by fumonisins. Implications for diseases associated with fusarium moniliforme. *J. Biol. Chem.* 266, 14486–14490.
- Wang, N., Wu, W., Pan, J., Long, M., 2019. Detoxification strategies for Zearalenone using microorganisms: a review. *Microorg* 7, 208. <https://doi.org/10.3390/MICROORGANISMS7070208> (2019, Vol. 7, Page 208).
- Wang, B., Tsakiridis, E.E., Zhang, S., Llanos, A., Desjardins, E.M., Yabut, J.M., Green, A.E., Day, E.A., Smith, B.K., Lally, J.S.V., Wu, J., Raphenya, A.R., Srinivasan, K.A., McArthur, A.G., Kajimura, S., Patel, J.S., Wade, M.G., Morrison, K.M., Holloway, A.C., Steinberg, G.R., 2021. The pesticide chlorpyrifos promotes obesity by inhibiting diet-induced thermogenesis in brown adipose tissue. *Nat. Commun.* 12, 1–12. <https://doi.org/10.1038/s41467-021-25384-y> (2021 121).
- Wangia-Dixon, R.N., Nishimwe, K., 2021. Molecular Toxicology and Carcinogenesis of Fumonisin: A Review. 39, pp. 44–67. <https://doi.org/10.1080/26896583.2020.1867449> (doi:10.1080/26896583.2020.1867449).
- World Health Organization, 2021. Obesity and overweight. <https://www.who.int/news-room/factsheets/detail/obesity-and-overweight> June.
- Xia, J.Y., Holland, W.L., Kusminski, C.M., Sun, K., Sharma, A.X., Pearson, M.J., Sifuentes, A.J., McDonald, J.G., Gordillo, R., Scherer, P.E., 2015. Targeted induction of ceramide degradation leads to improved systemic metabolism and reduced hepatic steatosis. *Cell Metab.* 22, 266–278. <https://doi.org/10.1016/J.CMET.2015.06.007>.
- Yu, S., Jia, B., Liu, N., Yu, D., Wu, A., 2020. Evaluation of the individual and combined toxicity of Fumonisin mycotoxins in human gastric epithelial cells. *Int. J. Mol. Sci.* 21, 5917. <https://doi.org/10.3390/ijms21165917>.
- Yueh, M.F., He, F., Chen, C., Vu, C., Tripathi, A., Knight, R., Karin, M., Chen, S., Tukey, R.H., 2020. Triclosan leads to dysregulation of the metabolic regulator FGF21 exacerbating high fat diet-induced nonalcoholic fatty liver disease. *Proc. Natl. Acad. Sci. U. S. A.* 117, 31259–31266. <https://doi.org/10.1073/PNAS.2017129117/-/DCSUPPLEMENTAL>.